b-tagging in DELPHI at LEP

P. Abreu, W. Adam, T. Adye, P. Adzic, T. Albrecht, T. Alderweireld, R. Alemany-Fernandez, T. Allmendinger, P.P. Allport, S. Almehed, et al.

EUROPEAN ORGANIZATION FOR NUCLEAR RESEARCH

CERN–EP/2002-088

2 October 2002

b-tagging in DELPHI at LEP

DELPHI Collaboration

Abstract

The standard method used for tagging b-hadrons in the DELPHI experiment at the CERN LEP Collider is discussed in detail. The main ingredient of b-tagging is the impact parameters of tracks, which relies mostly on the vertex detector. Additional information, such as the mass of particles associated to a secondary vertex, significantly improves the selection efficiency and the background suppression. The paper describes various discriminating variables used for the tagging and the procedure of their combination. In addition, applications of b-tagging to some physics analyses, which depend crucially on the performance and reliability of b-tagging, are described briefly.

(Accepted by Eur. Phys. J. C)

J.Abdallah[26], P.Abreu[24], W.Adam[54], T.Adye[38], P.Adzic[12], T.Albrecht[19], T.Alderweireld[2], R.Alemany-Fernandez[8], T.Allmendinger[19], P.P.Allport[25], S.Almehed[27], U.Amaldi[30], N.Amapane[47], S.Amato[51], E.Anashkin[37], A.Andreazza[29], S.Andringa[24], N.Anjos[24], P.Antilogus[28], W-D.Apel[19], Y.Arnoud[16], S.Ask[27], B.Asman[46], J.E.Augustin[26], A.Augustinus[8], P.Baillon[8], A.Ballestrero[48], P.Bambade[22], R.Barbier[28], D.Bardin[18], G.Barker[19], A.Baroncelli[40], M.Bates[38], M.Battaglia[8], M.Baubillier[26], K-H.Becks[56], M.Begalli[6], A.Behrmann[56], N.Benekos[33], A.Benvenuti[5], C.Berat[16], M.Berggren[26], L.Berntzon[46], D.Bertrand[2], M.Besancon[42], N.Besson[42], J.Bibby[36], P.Biffi[29], D.Bloch[9], M.Blom[32], M.Bonesini[30], M.Boonekamp[42], P.S.L.Booth[25], G.Borisov[23], O.Botner[52], B.Bouquet[22], T.J.V.Bowcock[25], I.Boyko[18], M.Bracko[45], P.Branchini[40], R.Brenner[52], E.Brodet[36], P.Bruckman[20], J.M.Brunet[7], L.Bugge[34], P.Buschmann[56], M.Caccia[29,10], M.Calvi[30], T.Camporesi[8], V.Canale[39], F.Carena[8], N.Castro[24], F.Cavallo[5], V.Chabaud[8], M.Chapkin[44], Ph.Charpentier[8], P.Checchia[37], R.Chierici[8], P.Chliapnikov[44], J.Chudoba[8], S.U.Chung[8], K.Cieslik[20], P.Collins[8], R.Contri[15], G.Cosme[22], F.Cossutti[50], M.J.Costa[53], F.Couchot[22], B.Crawley[1], D.Crennell[38], J.Cuevas[35], B.D'Almagne[22], J.D'Hondt[2], J.Dalmau[46], T.da Silva[51], W.Da Silva[26], G.Della Ricca[50], A.De Angelis[50], W.De Boer[19], C.De Clercq[2], B.De Lotto[50], N.De Maria[47], A.De Min[37], L.de Paula[51], L.Di Ciaccio[39], H.Dijkstra[8], A.Di Simone[40], K.Doroba[55], J.Drees[56,8], M.Dris[33], G.Eigen[4], T.Ekelof[52], M.Ellert[52], M.Elsing[8], M.C.Espirito Santo[8], G.Fanourakis[12], D.Fassouliotis[12], M.Feindt[19], J.Fernandez[43], A.Ferrer[53], F.Ferro[15], U.Flagmeyer[56], H.Foeth[8], E.Fokitis[33], F.Fulda-Quenzer[22], J.Fuster[53], M.Gandelman[51], C.Garcia[53], Ph.Gavillet[8], E.Gazis[33], T.Geralis[12], R.Gokieli[8,55], B.Golob[45], J.J.Gomez Cadenas[53,8], G.Gomez-Ceballos[43], P.Goncalves[24], E.Graziani[40], G.Grosdidier[22], K.Grzelak[55], J.Guy[38], C.Haag[19], A.Hallgren[52], K.Hamacher[56], K.Hamilton[36], J.Hansen[34], S.Haug[34], F.Hauler[19], V.Hedberg[27], M.Hennecke[19], J.A. Hernando[53], H.Herr[8], J.Heuser[56,41], S-O.Holmgren[46], P.J.Holt[8], M.A.Houlden[25], K.Hultqvist[46], J.N.Jackson[25], P.Jalocha[20], Ch.Jarlskog[27], G.Jarlskog[27], P.Jarry[42], D.Jeans[36], E.K.Johansson[46], P.D.Johansson[46], P.Jonsson[28], C.Joram[8], L.Jungermann[19], F.Kapusta[26], M.Karlsson[46], S.Katsanevas[28], E.Katsoufis[33], R.Keranen[19], G.Kernel[45], B.P.Kersevan[8,45], A.Kiiskinen[17], B.T.King[25], N.J.Kjaer[8], P.Kluit[32], P.Kokkinias[12], C.Kourkoumelis[3], O.Kouznetsov[18], Z.Krumstein[18], M.Kucharczyk[20], W.Kucewicz[20], J.Kurowska[55], J.Lamsa[1], G.Leder[54], F.Ledroit[16], L.Leinonen[46], R.Leitner[31], J.Lemonne[2], V.Lepeltier[22], T.Lesiak[20], W.Liebig[56], D.Liko[54], A.Lipniacka[46], J.H.Lopes[51], J.M.Lopez[35], D.Loukas[12], P.Lutz[42], L.Lyons[36], J.MacNaughton[54], A.Malek[56], S.Maltezos[33], F.Mandl[54], J.Marco[43], R.Marco[43], B.Marechal[51], M.Margoni[37], J-C.Marin[8], C.Mariotti[8], A.Markou[12], C.Martinez-Rivero[43], F.Martinez-Vidal[53], J.Masik[14], N.Mastroyiannopoulos[12], F.Matorras[43], C.Matteuzzi[30], F.Mazzucato[37], M.Mazzucato[37], R.Mc Nulty[25], C.Meroni[29], W.T.Meyer[1], E.Migliore[47], W.Mitaroff[54], U.Mjoernmark[27], T.Moa[46], M.Moch[19], K.Moenig[8,11], R.Monge[15], J.Montenegro[32], D.Moraes[51], S.Moreno[24], P.Morettini[15], U.Mueller[56], K.Muenich[56], M.Mulders[32], L.Mundim[6], W.Murray[38], B.Muryn[21], G.Myatt[36], T.Myklebust[34], M.Nassiakou[12], F.Navarria[5], K.Nawrocki[55], R.Nicolaidou[42], P.Niezurawski[55], M.Nikolenko[18,9], A.Nomerotski[37,13], A.Norman[36], A.Nygren[27], A.Oblakowska-Mucha[21], V.Obraztsov[44], A.Olshevski[18], A.Onofre[24], R.Orava[17], K.Osterberg[17], A.Ouraou[42], A.Oyanguren[53], M.Paganoni[30], S.Paiano[5], J.P.Palacios[25], H.Palka[20], Th.D.Papadopoulou[33], L.Pape[8], C.Parkes[25], F.Parodi[15], U.Parzefall[8], A.Passeri[40], O.Passon[56], L.Peralta[24], V.Perepelitsa[53], A.Perrotta[5], A.Petrolini[15], J.Piedra[43], L.Pieri[40], F.Pierre[42], M.Pimenta[24], E.Piotto[8], T.Podobnik[45], V.Poireau[42], M.E.Pol[6], G.Polok[20], P.Poropat[†50], V.Pozdniakov[18], N.Pukhaeva[2,18], A.Pullia[30], J.Rames[14], L.Ramler[19], A.Read[34], P.Rebecchi[8], J.Rehn[19], D.Reid[32], R.Reinhardt[56], P.Renton[36], F.Richard[22], J.Ridky[14], M.Rivero[43], D.Rodriguez[43], A.Romero[47], P.Ronchese[37], E.Rosenberg[1], P.Roudeau[22], T.Rovelli[5], V.Ruhlmann-Kleider[42], D.Ryabtchikov[44], A.Sadovsky[18], L.Salmi[17], J.Salt[53], A.Savoy-Navarro[26], U.Schwickerath[8], A.Segar[36], R.Sekulin[38], M.Siebel[56], A.Sisakian[18], G.Smadja[28], O.Smirnova[27], A.Sokolov[44], A.Sopczak[23], R.Sosnowski[55], T.Spassov[8], M.Stanitzki[19], I.Stavitski[37,25], A.Stocchi[22], J.Strauss[54], B.Stugu[4], M.Szczekowski[55], M.Szeptycka[55], T.Szumlak[21], T.Tabarelli[30], A.C.Taffard[25], F.Tegenfeldt[52], J.Timmermans[32], N.Tinti[5], L.Tkatchev[18], M.Tobin[25], S.Todorovova[14], A.Tomaradze[8], B.Tome[24], A.Tonazzo[30], P.Tortosa[53], P.Travnicek[14], D.Treille[8], W.Trischuk[49], G.Tristram[7], M.Trochimczuk[55], C.Troncon[29], M-L.Turluer[42], I.A.Tyapkin[18], P.Tyapkin[18], M.Tyndel[38], S.Tzamarias[12], V.Uvarov[44], G.Valenti[5], P.Van Dam[32], J.Van Eldik[8], A.Van Lysebetten[2], N.van Remortel[2], I.Van Vulpen[32], G.Vegni[29], F.Veloso[24], W.Venus[38], F.Verbeure[†2], P.Verdier[28], V.Verzi[39], D.Vilanova[42], L.Vitale[50], V.Vrba[14], H.Wahlen[56], A.J.Washbrook[25], P.Weilhammer[8], C.Weiser[19], D.Wicke[8],

J.Wickens[2], G.Wilkinson[36], M.Winter[9], M.Witek[20], O.Yushchenko[44], A.Zalewska[20], P.Zalewski[55], D.Zavrtanik[45], N.I.Zimin[18], A.Zintchenko[18], M.Zupan[12]

[1]Department of Physics and Astronomy, Iowa State University, Ames IA 50011-3160, USA
[2]Physics Department, Universiteit Antwerpen, Universiteitsplein 1, B-2610 Antwerpen, Belgium
and IIHE, ULB-VUB, Pleinlaan 2, B-1050 Brussels, Belgium
and Faculté des Sciences, Univ. de l'Etat Mons, Av. Maistriau 19, B-7000 Mons, Belgium
[3]Physics Laboratory, University of Athens, Solonos Str. 104, GR-10680 Athens, Greece
[4]Department of Physics, University of Bergen, Allégaten 55, NO-5007 Bergen, Norway
[5]Dipartimento di Fisica, Università di Bologna and INFN, Via Irnerio 46, IT-40126 Bologna, Italy
[6]Centro Brasileiro de Pesquisas Físicas, rua Xavier Sigaud 150, BR-22290 Rio de Janeiro, Brazil
and Depto. de Física, Pont. Univ. Católica, C.P. 38071 BR-22453 Rio de Janeiro, Brazil
and Inst. de Física, Univ. Estadual do Rio de Janeiro, rua São Francisco Xavier 524, Rio de Janeiro, Brazil
[7]Collège de France, Lab. de Physique Corpusculaire, IN2P3-CNRS, FR-75231 Paris Cedex 05, France
[8]CERN, CH-1211 Geneva 23, Switzerland
[9]Institut de Recherches Subatomiques, IN2P3 - CNRS/ULP - BP20, FR-67037 Strasbourg Cedex, France
[10]Now at Universita dell'Insubria in Como, Dip.to di Scienze CC.FF.MM' via Vallegio 11, 1-22100 Como, Italy
[11]Now at DESY-Zeuthen, Platanenallee 6, D-15735 Zeuthen, Germany
[12]Institute of Nuclear Physics, N.C.S.R. Demokritos, P.O. Box 60228, GR-15310 Athens, Greece
[13]Now at Fermilab (FNAL), Kirk and Pine Streets, P.O. Box 500, Batavia, IL 60510
[14]FZU, Inst. of Phys. of the C.A.S. High Energy Physics Division, Na Slovance 2, CZ-180 40, Praha 8, Czech Republic
[15]Dipartimento di Fisica, Università di Genova and INFN, Via Dodecaneso 33, IT-16146 Genova, Italy
[16]Institut des Sciences Nucléaires, IN2P3-CNRS, Université de Grenoble 1, FR-38026 Grenoble Cedex, France
[17]Helsinki Institute of Physics, HIP, P.O. Box 9, FI-00014 Helsinki, Finland
[18]Joint Institute for Nuclear Research, Dubna, Head Post Office, P.O. Box 79, RU-101 000 Moscow, Russian Federation
[19]Institut für Experimentelle Kernphysik, Universität Karlsruhe, Postfach 6980, DE-76128 Karlsruhe, Germany
[20]Institute of Nuclear Physics,Ul. Kawiory 26a, PL-30055 Krakow, Poland
[21]Faculty of Physics and Nuclear Techniques, University of Mining and Metallurgy, PL-30055 Krakow, Poland
[22]Université de Paris-Sud, Lab. de l'Accélérateur Linéaire, IN2P3-CNRS, Bât. 200, FR-91405 Orsay Cedex, France
[23]School of Physics and Chemistry, University of Landcaster, Lancaster LA1 4YB, UK
[24]LIP, IST, FCUL - Av. Elias Garcia, 14-1^{o}, PT-1000 Lisboa Codex, Portugal
[25]Department of Physics, University of Liverpool, P.O. Box 147, Liverpool L69 3BX, UK
[26]LPNHE, IN2P3-CNRS, Univ. Paris VI et VII, Tour 33 (RdC), 4 place Jussieu, FR-75252 Paris Cedex 05, France
[27]Department of Physics, University of Lund, Sölvegatan 14, SE-223 63 Lund, Sweden
[28]Université Claude Bernard de Lyon, IPNL, IN2P3-CNRS, FR-69622 Villeurbanne Cedex, France
[29]Dipartimento di Fisica, Università di Milano and INFN-MILANO, Via Celoria 16, IT-20133 Milan, Italy
[30]Dipartimento di Fisica, Univ. di Milano-Bicocca and INFN-MILANO, Piazza della Scienza 2, IT-20126 Milan, Italy
[31]IPNP of MFF, Charles Univ., Areal MFF, V Holesovickach 2, CZ-180 00, Praha 8, Czech Republic
[32]NIKHEF, Postbus 41882, NL-1009 DB Amsterdam, The Netherlands
[33]National Technical University, Physics Department, Zografou Campus, GR-15773 Athens, Greece
[34]Physics Department, University of Oslo, Blindern, NO-0316 Oslo, Norway
[35]Dpto. Fisica, Univ. Oviedo, Avda. Calvo Sotelo s/n, ES-33007 Oviedo, Spain
[36]Department of Physics, University of Oxford, Keble Road, Oxford OX1 3RH, UK
[37]Dipartimento di Fisica, Università di Padova and INFN, Via Marzolo 8, IT-35131 Padua, Italy
[38]Rutherford Appleton Laboratory, Chilton, Didcot OX11 OQX, UK
[39]Dipartimento di Fisica, Università di Roma II and INFN, Tor Vergata, IT-00173 Rome, Italy
[40]Dipartimento di Fisica, Università di Roma III and INFN, Via della Vasca Navale 84, IT-00146 Rome, Italy
[41]Now at Inst. of Physical and Chemical Research RIKEN, 2-1 Hirosawa, Wako-shi, Saitama 351-0198, Japan
[42]DAPNIA/Service de Physique des Particules, CEA-Saclay, FR-91191 Gif-sur-Yvette Cedex, France
[43]Instituto de Fisica de Cantabria (CSIC-UC), Avda. los Castros s/n, ES-39006 Santander, Spain
[44]Inst. for High Energy Physics, Serpukov P.O. Box 35, Protvino, (Moscow Region), Russian Federation
[45]J. Stefan Institute, Jamova 39, SI-1000 Ljubljana, Slovenia and Laboratory for Astroparticle Physics,
Nova Gorica Polytechnic, Kostanjeviska 16a, SI-5000 Nova Gorica, Slovenia,
and Department of Physics, University of Ljubljana, SI-1000 Ljubljana, Slovenia
[46]Fysikum, Stockholm University, Box 6730, SE-113 85 Stockholm, Sweden
[47]Dipartimento di Fisica Sperimentale, Università di Torino and INFN, Via P. Giuria 1, IT-10125 Turin, Italy
[48]INFN,Sezione di Torino, and Dipartimento di Fisica Teorica, Università di Torino, Via P. Giuria 1,
IT-10125 Turin, Italy
[49]Now at Institute of Particule Physics of Canada, Univ. of Toronto, Toronto, Ontario, Canada M5S1A7
[50]Dipartimento di Fisica, Università di Trieste and INFN, Via A. Valerio 2, IT-34127 Trieste, Italy
and Istituto di Fisica, Università di Udine, IT-33100 Udine, Italy
[51]Univ. Federal do Rio de Janeiro, C.P. 68528 Cidade Univ., Ilha do Fundão BR-21945-970 Rio de Janeiro, Brazil
[52]Department of Radiation Sciences, University of Uppsala, P.O. Box 535, SE-751 21 Uppsala, Sweden
[53]IFIC, Valencia-CSIC, and D.F.A.M.N., U. de Valencia, Avda. Dr. Moliner 50, ES-46100 Burjassot (Valencia), Spain

[54]Institut für Hochenergiephysik, Österr. Akad. d. Wissensch., Nikolsdorfergasse 18, AT-1050 Vienna, Austria
[55]Inst. Nuclear Studies and University of Warsaw, Ul. Hoza 69, PL-00681 Warsaw, Poland
[56]Fachbereich Physik, University of Wuppertal, Postfach 100 127, DE-42097 Wuppertal, Germany
† deceased

1 Introduction

The study of heavy b- and c- quarks is one of the most interesting subjects in experimental High Energy Physics, directly related to the verification of the Standard Model (SM) and the search for its possible violations. Where these may occur is very model-dependent, but it may well be that the third generation particles will provide some important clues to new effects. This is a large part of the motivation for studying b-quarks at LEP, where top-quark pair production is kinematically inaccessible. It is thus important to have algorithms for selecting events with b-quarks while keeping backgrounds small. Efficiency and purity or background rejection are important parameters of these techniques. Because searches for such deviations from the SM often involve precision measurements, it is crucial to have a very well understood and monitored b-tagging algorithm.

A further reason for selecting b-quarks is the search for the Higgs boson. For the SM Higgs with mass of relevance for LEP and the Tevatron, the predominant decay mode is to $b\bar{b}$ pairs. Thus tagging b-jets provides a valuable means of selecting candidates while reducing backgrounds to low levels, thereby enabling searches to achieve high sensitivity.

In this paper the b-tagging technique developed for the DELPHI experiment at the LEP electron-positron collider is described. LEP ran at centre-of-mass energies around the Z (91 GeV) over the period 1989 to 1995, and then at higher energies up to 208 GeV, before being turned off in 2000. Much of the technique used here would be applicable, with suitable modifications, in other experimental situations.

The lifetimes of b-hadrons are around 1.6 ps. This means that flight distances are of order 3 mm for a 35 GeV b-hadron, this being a typical energy in a 2-jet event at the Z, or in a 4-jet event at LEP2 energies. Correspondingly the decay tracks from a b-hadron have non-zero impact parameters[1], i.e. when extrapolated backward in space they do not pass exactly through the beam interaction region. The scale of these impact parameters is $c\tau \approx 400$ μm. This is to be compared with the DELPHI experimental resolution σ of about

$$\sigma = 27 \oplus 63/(p \sin^{3/2}\theta)\,\mu\mathrm{m} \tag{1}$$

where p and θ are the momentum (in GeV/c) and the polar angle of the track. The symbol $\oplus$ denotes the quadratic sum of terms. Eqn. (1) is for the impact parameter (IP) in the plane perpendicular to the beam; along the beam direction, the resolution is slightly worse. Because the micro-vertex detector is crucial for achieving this accuracy in IP measurements, it is described in Section 2.

The impact parameters provide the main variable for b-tagging. For all the tracks in a jet, the observed impact parameters and resolutions are combined into a single variable, the lifetime probability, which measures the consistency with the hypothesis that all tracks come directly from the primary vertex. For events without long-lived particles, this variable should be uniformly distributed between zero and unity. In contrast, for b-jets it has predominantly small values. Details of how this variable is constructed are elaborated in Section 3.

Other features of the event are also sensitive to b-quarks, and some of them are also used together with the IP information to construct a 'combined tag'. For example, b-hadrons have a 10% probability of decaying to electrons or muons, and these often have a transverse momentum with respect to the b-jet axis of around 1 GeV/c or larger. On its own, the high-p_T lepton tag would have too low an efficiency for many b-quark studies, but the presence of such a lepton is useful information to combine with the IP measurements. The combined tag also makes use of other variables which have significantly different

[1] See Section 3.1 for more detailed definitions and discussion of impact parameters.

distributions for b-quark and for other events, e.g. the charged particle rapidities with respect to the jet axis. Further details on these variables and the way in which they are combined are given in Section 4. The combined tag including the lifetime probability and secondary vertex mass, rapidities and fractional energy (described in Section 4.3) was used for the measurements at the Z (see Sections 6.1 – 6.4). For most LEP2 b-tagging analyses, the transverse momentum missing at the secondary vertex and the transverse momentum with respect to the jet axis of any electron or muon were also used in the combination.

The combination method used is optimal for uncorrelated variables. The extent to which it is possible to improve on the 'combined tag', for example by using extra information such as the jet energy, is investigated in Section 4.6. The resulting 'equalised tag' was used in the Higgs search at LEP2 (see Section 6.5).

Section 5 contains some technical aspects of the b-tagging. In particular it describes some modifications that were required to the physics generators of the Monte Carlo simulation.

Finally, some physics studies for which b-tagging plays a crucial role are outlined in Section 6. First there is the measurement of the fraction of hadronic Z decays which contain b-quarks (see Section 6.1). A precise measurement of this quantity requires high efficiency tagging, while keeping down the backgrounds from other quarks in order to reduce the systematic errors. This is followed by applications of b-tagging to the measurement of the production rate of events with 4 b-jets, and of the b-hadron charged decay multiplicity. Section 6.4 describes a measurement of the b-fraction in 3-jet events, which is sensitive to the mass of the b-quark. This uses anti b-tagging to select light quark events. Finally the crucial reliance on b-tagging of the search for the Higgs is described in Section 6.5.

2 The DELPHI Vertex Detector

2.1 Overview

The silicon vertex detectors of the DELPHI experiment have undergone various upgrades throughout the lifetime of the experiment. For the statistics collected in 1991-1993 it provided measurements in the transverse ($R\phi$) plane[2] only [1].

The DELPHI Double Sided Vertex Detector (DSVD) [2] was installed in the experiment in early 1994 and by the end of the Z running at LEP had contributed to the reconstruction and analysis of approximately 2 million Z decays. Two of its three layers were equipped with double-sided orthogonal readouts, thereby upgrading the IP and vertexing capabilities by adding information from the longitudinal (Rz) plane. The extra coordinate helps to associate tracks to vertices where the single $R\phi$ view alone might have ambiguities. This upgrade led to about a 30% improvement in the b-tagging efficiency at fixed purity. The geometrical layout of the DSVD is shown in figure 1. The three layers, termed Closer, Inner, and Outer, were at average radii of 6.3, 9.0 and 10.9 cm respectively, with the Outer and Closer layers instrumented with the double-sided orthogonal readout. The three-layer polar angular coverage was between 44° and 136°, with the Closer Layer providing additional coverage in anticipation of the subsequent SiT upgrade described below. The transverse view displays the large degree of overlap (up to

[2]DELPHI uses a cylindrical polar co-ordinate system, with the z axis along the beam direction (and the magnetic field axis). R and ϕ are the radial and azimuthal co-ordinates in the transverse plane, θ is the polar angle with respect to the beam axis. The Cartesian co-ordinates x and y are horizontal and vertical respectively.

20% of the sensitive region in the Inner Layer), which was an important ingredient for the alignment. The average thickness of each silicon module was 0.5% of a radiation length. The z readout was routed via an integrated double metal layer, thus adding negligible extra material in the barrel region, and helping to keep multiple scattering to a minimum.

The DELPHI Silicon Tracker (SiT) [3] was a further upgrade for the physics requirements at LEP2, and the barrel part relevant for b-tagging was fully installed in 1996. Physics objectives of LEP2, such as the measurement of four-fermion processes and the searches for the Higgs boson or for super-symmetric particles, required a larger polar angle coverage than at LEP1. The design goal was to achieve an equivalent b-tagging performance to the DELPHI DSVD, and in addition to extend this to around 25° in θ, after which the b-tagging capabilities were limited by multiple scattering in the beam-pipe. The SiT also incorporated end-caps of mini-strip and pixel detectors for tracking in the forward region [3, 4]. The geometrical layout of the SiT is shown in figure 2. The radii of the layers were similar to the DSVD, but the Outer and Inner layers were doubled in length to provide the extra angular coverage. The Closer Layer was double-sided, the Inner Layer was double-sided for $21° < \theta < 44°$ (and the corresponding backward region) and single-sided in the centre, and the Outer Layer provided $R\phi$ and Rz measurements from its crossed detector arrangement [3]. The impact of this detector on b-tagging is shown in figure 3.

2.2 Alignment and Performance

b-tagging quality relies on excellent alignment of the vertex detector. The starting point of the alignment was the information from an optical and mechanical survey before installation. This was refined with the information from tracks from Z decays, using a stand-alone procedure where the momentum of the track was the only information taken from the rest of the DELPHI detector. The precision of the vertex detector hits has allowed a number of important effects to be identified, including some common to all LEP vertex detectors and certain previously unmeasured properties of silicon detectors. They include:

- coherent deformations, such as a torsion or shear of the entire structure;
- bowing of the silicon modules due to the different response of the silicon and the module support to changes in temperature and humidity;
- barycentric shift effects, whereby the centres of gravity of the charge clouds of electrons and holes in the silicon do not correspond to the mid-plane of the detector, nor to each other;
- acollinearity of the LEP electron and positron beams leading to lepton pairs from Z decays which cannot be assumed to be back-to-back in the alignment procedure.

More details can be found in [5]. The precise vertex detector alignment has also led to better understanding of other detectors, such as the TPC, the track distortions of which were corrected.

The ultimate performance of the vertex detector with respect to b-tagging can be measured by the IP resolution, which in the $R\phi$ plane can be parametrised by:

$$\sigma_{R\phi} \;=\; 27 \oplus \frac{63}{\mathrm{p}\,\sin^{\frac{3}{2}}\theta}\;\mu\mathrm{m} \qquad (2)$$

with p in GeV/c. The IP resolution in the Rz plane for two typical θ regions can be parametrised by:

$$\sigma_{Rz} = 39 \oplus \frac{71}{\mathrm{p}}\ \mu\mathrm{m}\ (\text{for } 80^\circ < \theta < 90^\circ) \quad (3)$$

$$\sigma_{Rz} = 96 \oplus \frac{151}{\mathrm{p}}\ \mu\mathrm{m}\ (\text{for } 45^\circ < \theta < 55^\circ), \quad (4)$$

These equations are the quadratic sums of a constant and a momentum dependent term, corresponding to the intrinsic resolution and to the multiple scattering contributions respectively. For tracks coming from b-decays, these contributions are of similar magnitude. Typical distributions of the IP resolutions as functions of momenta are shown in figure 4.

3 Lifetime Tagging

b-hadrons in many aspects are significantly different from all other particles. They have a long lifetime, large mass, high decay multiplicity, substantial leptonic branching rate, etc. The most important property for the selection of b-hadrons is their lifetime. Among the main features of lifetime tagging are a simple and transparent definition and ease of control, since it relies on a single measured quantity, the track IP.

In this section the definition of the main elements entering in the lifetime tagging together with the principles of its construction are given. This tagging itself provides efficient separation of the b-quark from other flavours, which is further enhanced by including additional variables (see Section 4). The method of lifetime tagging used by DELPHI was originally proposed by the ALEPH collaboration [6].

3.1 Impact Parameter

The general 3-dimensional IP is the minimal distance between the estimated primary interaction point and the track trajectory. The decay of a long-lived particle produces tracks with large impact parameters, which is not the case for particles from the primary interaction. Lifetime tagging is based on this difference.

For b-tagging in DELPHI, a slightly different approach is adopted, with a separation of the 3-dimensional information into $R\phi$ and Rz components. The IP component in the $R\phi$ plane is defined as the minimal distance between the primary vertex (PV) and the track trajectory projected onto the plane perpendicular to the beam direction. The point of the closest approach (P_C) of the track trajectory to the primary vertex in the $R\phi$ plane is also used to define the Rz component of the IP. This is the difference between the z-coordinates of the primary vertex and of the point P_C (see fig. 5).

According to these definitions, there are two ingredients in the IP computation: the parameters of the track trajectory, provided by the track fit, and the position of the primary interaction. The parameters of the track trajectory are the track direction given by its polar and azimuthal angles (θ, ϕ) at the point P_0 of the closest approach to the origin O; and ($\varepsilon_{R\phi}$, ε_{Rz}), the equivalent of the IP components but defined with respect to the origin O, rather than with respect to the primary vertex. The reconstruction of the primary vertex is explained in the next section. In the approximation that the tracks can be regarded as straight lines between P_0 and P_C, the IP components $d_{R\phi}$ and d_{Rz} with respect to the primary vertex position $\overrightarrow{V}$ are calculated as:

$$d_{R\phi} = \varepsilon_{R\phi} - (\overrightarrow{e} \cdot \overrightarrow{V}) \quad (5)$$

$$d_{Rz} = \varepsilon_{Rz} + \cot\theta(\overrightarrow{u} \cdot \overrightarrow{V}) - V_z = \varepsilon_{Rz} - (\overrightarrow{l} \cdot \overrightarrow{V}) \quad (6)$$

Here $\overrightarrow{u}$ is the unit vector along the track direction in the $R\phi$ plane: $\overrightarrow{u} = \{\cos\phi, \sin\phi, 0\}$; $\overrightarrow{e}$ is the unit vector perpendicular to the track direction in $R\phi$ plane: $\overrightarrow{e} = \{\sin\phi, -\cos\phi, 0\}$; and $\overrightarrow{l} = \{-\cot\theta\cos\phi, -\cot\theta\sin\phi, 1\}$. Figure 5 illustrates these definitions of the IP components.

The main reason for the separation of the 3-dimensional IP into $R\phi$ and Rz components is that the measurement of the particle trajectory in DELPHI is performed independently in these two planes with somewhat different precision (see eqns. (2) – (4)). Also the beam-spot is smaller in the transverse directions. In addition, there are 3 sensitive layers of vertex detector in the $R\phi$ plane and only 2 layers in the Rz plane; the fraction of tracks with wrong hit association in the Rz plane is thus higher. The separate treatment of the IP components provides the freedom to reject bad measurements in the Rz plane, while keeping useful $R\phi$ information. Finally, the data before 1994 were taken with the 2-dimensional vertex detector providing track measurements in the $R\phi$ plane only. The separate use of the $R\phi$ and Rz information is one of the crucial points of our tagging algorithm, significantly influencing its structure.

3.2 Primary Vertex

The primary vertex is reconstructed for each event using a set of selected tracks and the beam-spot position. The beam-spot is the zone of intersection of the two colliding beams of LEP. It has a small size in the $R\phi$ plane ($\sigma_x \simeq 150\mu$m, σ_y less than 10μm), while it is several millimetres long along the beam direction. It is relatively stable within a fill, and so can be used as a constraint for the primary vertex fit.

The beam-spot is measured using events which have a vertex formed by at least 3 tracks with hits in the silicon strip detectors. These vertices are used to fit the position in 3 dimensions and also the x and z size of the interaction region in time periods of around 20 minutes. The size of the interaction region in y is not fitted, because it is smaller than the corresponding position error, and the value $\sigma_y = 10$ μm is used.

The PV position is obtained by minimising the χ^2 function:

$$\chi^2(\overrightarrow{V}) = \sum_a \sum_{\alpha,\beta=1,2} d^a_\alpha (S_a^{-1})_{\alpha\beta} d^a_\beta + \sum_i \frac{(V_i^{sp} - V_i)^2}{(\sigma_i^{sp})^2} \quad (7)$$

Here $\{d^a_1, d^a_2\} = \{d^a_{R\phi}, d^a_{Rz}\}$ is the 2-dimensional vector of IP components for each track a entering in the PV fit and S_a is the covariance matrix of the measured quantities $\{\varepsilon^a_{R\phi}, \varepsilon^a_{Rz}\}$; since measurements in the $R\phi$ and Rz planes are made independently, the matrix S_a is almost diagonal. V_i^{sp} and σ_i^{sp} are the beam-spot position and size for the x and y coordinates. The first summation in equation (7) runs over all tracks selected for the PV fit. Because of our definitions (5-6) of the IP components, the dependence of χ^2 on the vertex position $\overrightarrow{V}$ is quadratic and hence the minimisation of (7) can be performed analytically.

An important part of the PV reconstruction is the selection of tracks and the rejection of bad measurements. Tracks with wrong hit associations in the vertex detector, as well

as those coming from decays of long-lived particles or from interactions in the detector material, bias the fitted PV position and a special rejection procedure attempts to reduce this bias.

For the PV computation, tracks with at least two $R\phi$ measurements and at least one Rz measurement are selected. First the fit using all these tracks (N_{tr}) is performed and $\chi^2(N_{tr})$ is computed. After that each track i is consecutively removed and the corresponding $\chi^2_i(N_{tr}-1)$ is obtained. The track i giving the maximal difference $\chi^2(N_{tr})-\chi^2_i(N_{tr}-1)$ is excluded from the fit if this difference exceeds a threshold value Δ, which was set to 6. This procedure is repeated while there are tracks with a χ^2 difference exceeding Δ. Since the beam-spot position constraint is used for the PV computation, all tracks may be rejected for some events. In this case the PV coincides with the beam-spot and its covariance matrix corresponds to the beam-spot size. The fraction of such events is about 1% for Z hadronic events.

This fitting procedure gives an average precision of the PV position for $q\bar{q}$ (where $q = uds$), $c\bar{c}$, $b\bar{b}$ simulated Z hadronic decays of $\sigma_x = 36, 44, 60$ μm and $\sigma_z = 43, 50, 70$ μm respectively, although the actual precision depends strongly on the number of tracks. The somewhat degraded precision for $b\bar{b}$ events is explained by the smaller multiplicity of primary tracks and by tracks from b-hadron decay occasionally included in the primary vertex.

3.3 Error and Sign of Impact Parameter

Since the PV position is used in the definition of an IP, the impact parameters of all tracks included in the PV fit are correlated with each other; their correlation coefficient is about 0.2. From equations (5-7) and the standard error propagation formalism, the error on the $R\phi$ IP is given by:

$$\sigma^2_{R\phi} = \begin{cases} (\sigma^{tr}_{R\phi})^2 - (\sigma^{pv}_{R\phi})^2 & \text{if the track is included in the PV fit} \\ (\sigma^{tr}_{R\phi})^2 + (\sigma^{pv}_{R\phi})^2 & \text{otherwise} \end{cases} \tag{8}$$

with similar equations for σ^2_{Rz}. Here $\sigma^{tr}_{R\phi}$ (σ^{tr}_{Rz}) is the error on $\varepsilon_{R\phi}$ (ε_{Rz}) coming from the track fit and σ^{pv} is the error from the PV fit, and includes implicitly the influence of all other impact parameters. More explicitly:

$$(\sigma^{pv}_{R\phi})^2 = \sum_{i,j} e_i S^V_{ij} e_j \tag{9}$$

$$(\sigma^{pv}_{Rz})^2 = \sum_{i,j} l_i S^V_{ij} l_j \tag{10}$$

where S^V_{ij} is the covariance matrix of the primary vertex fit, $\overrightarrow{e}$ and $\overrightarrow{l}$ are defined in Section 3.1, and repeated indices imply summation. The simplicity of the final equations is a consequence of our choice of IP components.

Using equations (5, 6 and 8) the track significances $S_{R\phi}$ and S_{Rz} are defined simply as:

$$S_{R\phi} = d_{R\phi}/\sigma_{R\phi} \tag{11}$$

$$S_{Rz} = d_{Rz}/\sigma_{Rz} \tag{12}$$

The track significance thus compares the measured value of the IP with its expected precision. This quantity is used as an input variable for the lifetime tagging. Tracks from

decays of long-lived particles (τ's, b-, c- and s-hadrons) often have large IPs, significantly exceeding $\sigma_{R\phi}$ and σ_{Rz}.

Equations (5-6) define the magnitude of IP components and their *geometrical* sign, while in the b-tagging method and throughout this paper the *lifetime* sign for IP is used. It requires knowledge of the flight path of the long-lived particle. In the simplest case the flight path is approximated by the direction of the jet[3] to which the given particle belongs. Often the decay point of the long-lived particle can be reconstructed (see Section 4.2); in this case the flight direction is defined as the direction from the primary to the secondary vertex. As can be seen in fig. 6, this improves the measurement of the flight direction. The azimuthal angle precision becomes slightly better than that for the polar angle because the vertex detector is more precise in the $R\phi$ plane. To obtain the *lifetime* sign of the $R\phi$ and Rz IPs, the point of closest approach in space of the track to the estimated B-flight path is computed and the sign is set negative (positive) if this point is upstream (downstream) of the PV position. The significance is assigned the same sign as the IP.

With this definition, tracks from decays of long-lived particles have predominantly positive signs while tracks coming directly from the PV are equally likely to be positive or negative. For b-tagging, tracks with positive IP are used, thus reducing by half the number of background tracks.

The distributions of positive and negative $R\phi$ significance are shown in fig. 7. The excess of positively signed tracks with large significance is clearly seen.

3.4 Track Probability

The distribution of the negative track significance is determined mainly by tracks coming from the PV, including scatters in the detector material, tracks with wrong hit association etc, while the contribution of tracks coming from decays of long-lived particles is about 1%. This distribution can thus be used to define the probability $P(S^0)$ for a track from the PV to have the measured value of the modulus of its significance exceeding the value S^0. This function is obtained by integration of the probability density function of the negative significance $f(S)$ from S^0 to infinity and assuming that $P(S^0)$ is the same for primary tracks with either positive or negative significance:

$$P(S^0) = \int_{S^0}^{\infty} f(S)dS \tag{13}$$

By definition, tracks from the PV should have a flat distribution of $P(S^0)$ between 0 and 1, while tracks from decays of long-lived particles and with large positive values of S^0 have small values of $P(S^0)$, reflecting the small probability for tracks from the primary vertex to have such large values of the IP and hence of S^0. As an example, fig. 8 shows the distribution of $P(S^0_{R\phi})$ for tracks with positive IP. The peak at small values of $P(S^0_{R\phi})$ is produced mainly by the long-lived particles. The transformation from significance to track probability is referred to as the calibration of the detector resolution.

For LEP1 analyses, the above calibration was performed using tracks from Z decays. At LEP2, there was the possibility of again using Z data for calibration; each year, short runs at the Z were taken before the start of and also interspersed with the high energy running. Alternatively, the calibration could be carried out using the same type of data as used to perform the relevant physics analysis. Thus for the Higgs search of Section 6.5, 4-jet events were also used for calibration in the channel where the H and Z both

[3]The default jet clustering algorithm is JADE, with y_{cut} set at 0.01. However, the user of the b-tagging package has the option of using any jet algorithm.

decay to 2 jets, while in the corresponding channel where the Z decays to two neutrinos, calibration was performed using '2-jets + missing energy' events. The use of calibration samples closely related to the data sample in principle allows for the following possible effects:

- because of possible movements of the relative positions of the different parts of the vertex detector with respect to the rest of DELPHI, the calibration could be time-dependent;
- track confusion and lifetime-signing (and hence calibration) could depend on the event topology;
- the IP resolution changes with polar angle θ. The jet distribution in θ depends on the particular physical process considered;
- the IP resolution is also energy dependent. The jet and track energy spectra depend on the physical process.

The calibration was performed separately for categories of tracks with different lifetime sensitivities. The categories were determined by the number of associated VD hits. A small number of VD hits associated with a track is often caused by incorrect reconstruction, and the significance distribution of such tracks has a larger non-Gaussian tail. By using a different track probability for them, this difference was taken into account. This approach was also used for the analysis of the data collected in 2000, when one out of the 12 sectors of the TPC was not operational during the last part of the data taking; tracks reconstructed without the TPC have worse precision, which requires using a separate track probability for them.

Another property of the track probability is that it can be defined directly from the data. This is very important, in that it allows the calibration of the detector resolution independently of the simulation. Such calibration allows to take into account possible differences between data and simulation. As a consequence, it also reduces the systematics due to detector effects in physics measurements.

For the construction of $P(S^0)$ it is important to reduce the contribution of tracks coming from the decay of long-lived particles. Using the negative significance distribution partially solves this problem. Additional suppression of the lifetime information is achieved by applying anti-b tagging to the event sample used for calibration. This anti-b tagging is based on tracks with positive IPs, and hence does not bias the negative significance distribution. The anti-b tagging reduces the fraction of $b\bar{b}$ events in the selected sample of hadronic Z events from 21.6% to less than 5% and the contribution of tracks from decays of b-hadrons is reduced correspondingly. Additional selection criteria for tracks used for calibration decrease the contribution from the decay products of light long-lived hadrons (K^0, hyperons) and hence reduce the tail of the significance distribution. They are specified in the next section.

3.5 Lifetime Probability

Track probabilities are directly used to construct a lifetime probability [6]. For any group of N tracks it is defined as:

$$P_N = \Pi \cdot \sum_{j=0}^{N_{R\phi}+N_{Rz}-1} (-\log \Pi)^j / j!, \quad \text{where} \quad \Pi = \prod_{i=1}^{N_{R\phi}} P(S^i_{R\phi}) \cdot \prod_{i=1}^{N_{Rz}} P(S^i_{Rz}) \qquad (14)$$

Here $P(S^i_{R\phi})$, $P(S^i_{Rz})$ are the track probabilities and $N_{R\phi}$, N_{Rz} are the number of $R\phi$ and Rz IPs used in the tagging. The definition of P_N thus ignores the small off-diagonal

elements of the IP error matrix and the correlation between different IPs coming from the use of the common PV.

The variable P_N has a simple and straightforward definition and can be computed for any group of tracks (e.g. a jet, hemisphere or whole event) which makes it flexible and easily adjustable to different physics applications. No other combination of IP measurements was found to give a better selection of b-quarks.

An attractive feature of lifetime tagging is that it is constructed using only the track IPs. This provides the possibility of achieving a good description of the b-tagging efficiency by the accurate tuning of the track resolution in simulation, as described in Section 3.6. It allows a significant decrease in the systematic uncertainties due to detector effects in physics measurements.

The meaning of the variable P_N is very similar to that of track probability $P(S)$: it is the probability for N tracks coming from the PV to have the product of their track probabilities exceeding the observed value. It varies between 0 and 1 and has a flat distribution for any group of N uncorrelated tracks coming from the PV. The contribution of tracks from secondary decays shifts P_N to lower values, producing a peak near 0.

The flat distribution of P_N for primary tracks can be verified by computing P_N^- for the sample of all tracks with negative impact parameters in anti-b tagged events. As explained in Section 3.4, the contribution of tracks from decays of long-lived particles in such a sample is small. The distribution of P_N^- is shown as the dotted curve in fig. 9. It is relatively flat, although there is a small peak near zero. This peak is produced by tracks from decays of long-lived particles, which are occasionally assigned to have negative IPs because of the error in their flight direction estimate. However, the value of this excess is significantly less than the peak in the distribution of P_N^+, computed using positive IPs. This distribution is shown as the solid curve in fig. 9. The latter peak is mainly produced by the $b\bar{b}$ events, as can be seen from fig. 9.

The separation of tracks into two samples depending on the sign of their IP is very important. The sample of negative IP tracks is used for the calibration of the detector resolution and the quality of this calibration is verified by the P_N^- distribution. In contrast, positive IP tracks are used for b-tagging. Thus the samples of tracks used in the calibration and in the analysis do not overlap. The P_N^- distribution also gives a good estimate of the background level from light quarks at the corresponding value of P_N^+.

The $R\phi$ and Rz components enter in eqn. (14) separately. As explained in Section 3.1, the fraction of wrong measurements in Rz is higher. Therefore, tighter selection criteria are applied to tracks for the Rz IP, and for some tracks only the $R\phi$ measurement is used. Thus, the separate treatment of IP components also allows the use of information which would otherwise be lost.

More specifically, the conditions applied to the tracks are as follows. All tracks with positive IP and at least one measurement in the VD are candidates for lifetime tagging. Tracks coming from reconstructed K^0 or Λ decays[4] are rejected. Both $R\phi$ and Rz IP components are required to be less than 0.2 cm, although this condition is removed if the track comes from a reconstructed secondary vertex (see Section 4.2).

One more parameter is used to provide additional suppression of bad Rz measurements. It is the distance D of closest approach in 3-dimensions between the track and the expected flight path of the long-lived particle, defined in the section 3.3. All tracks, both from the primary and secondary vertices, should have a small value of D provided the secondary vertex is close to the estimated flight direction. Therefore a large value of D with respect to its expected precision σ_D is used to identify wrong IP measurements.

[4]For V^0 reconstruction procedure see [7].

Rz IP measurements are rejected if D/σ_D exceeds 2.5. Both $R\phi$ and Rz measurements are excluded from lifetime tagging if D/σ_D exceeds 10.

Figure 10 shows the performance of the lifetime probability applied to simulated hadronic decays of the Z. The figure shows the efficiency of the b-quark selection versus the contamination of the selected sample by (u, d, s, c) flavours $(N_{udsc}/(N_{udsc}+N_b))$. The suppression of background flavours is shown for tagging of one jet (i.e. using only tracks from the given jet), and for the whole event. Event tagging is more efficient because b-quarks are produced in pairs.

b-tagging using only lifetime information is rather efficient and is sufficient for the needs of many physics applications. An important feature is its simple control of the tagging efficiency in simulation. Its performance is however substantially enhanced by including additional discriminating variables, such as the mass at the secondary vertex or the presence of energetic leptons. This method of 'combined b-tagging' is described in Section 4.

3.6 Tuning

Almost all precision measurements and searches for rare processes rely on a comparison of the observed data distributions with those predicted by a detailed simulation. For this comparison both the generation of the intrinsic physical processes and the simulation of detector response must be as realistic as possible. For the selection of events containing b-hadrons, the most important variables are the track IPs, therefore the description of the IP resolution can significantly influence the physics result and the value of the systematic uncertainty.

The generated events in the DELPHI experiment are processed by the detector simulation package [8] and the same reconstruction program [9] as for the data. For the simulation, the reconstruction program first applies some additional smearing to the reconstruction inputs to improve agreement with the particular data set being represented. For the vertex detector, this includes applying corrections for inefficient regions, adding noise hits, and randomly modifying the positions of the modules to simulate the effects of residual misalignments in the real data.

However, even after this procedure some disagreement between data and simulation in the track resolution description remains. This difference can be clearly seen, for example, in the distribution of the track significance (see fig. 11). Any disagreement in this quantity can result in a large discrepancy in the b-tagging description.

A detailed description of the method including the correction of the detector resolution in the $R\phi$ plane for the initial micro-vertex detector [1] is given in [10]. The application of this method for the tuning in the Rz plane for the DSVD at LEP1 and the SiT at LEP2 is similar and consists of the following steps:

- the appropriate parameterisations of the negative lifetime-signed IP ($d_{R\phi}$ and d_{Rz}) distributions are determined;
- the numerical coefficients for these parameterisations are extracted from the data;
- the errors of $d_{R\phi}$ and d_{Rz} given by the track fit are corrected both in data and in the simulation according to the parametrisation obtained while the correlation between $d_{R\phi}$ and d_{Rz} is not changed;
- additional smearing of $R\phi$ and Rz IPs in simulation is performed in order to reproduce the observed real data distributions.

The improvements in the significance description after applying this method can be seen in fig. 12. Fig. 13 shows the data to simulation ratio of the selection efficiency as

a function of the cut on the b-tagging variables. For the non-tuned version of b-tagging (dashed line) the difference between data and simulation is very significant for strong b-tagging cuts, corresponding to purer samples of B events. The tuning results in better agreement for both the lifetime and the combined b-tagging variables, the latter being described in the next section. The remaining differences between data and simulation can be explained by the uncertainties of the modelling of B decay and to a lesser extent its hadronic production.

This tuning procedure is incorporated in the b-tagging package and is used in all DELPHI measurements involving b-quark selection.

4 Combined Tagging

Efficient utilisation of different properties of b-hadrons requires the development of a technique for their combination into a single tagging variable. The simplest solution of applying some system of cuts on different discriminating variables, which was tried in other collaborations [11, 12], is not optimal due to a significant overlap between the signal and background for some of them. Instead, DELPHI uses a likelihood ratio method of variable combination [13, 14]. This approach has the important advantage of being technically very simple while at the same time providing powerful separation of signal and background. For independent variables, it gives optimal tagging, i.e. the best possible background suppression for a given signal efficiency [15]. It can easily be extended to any number of discriminating variables, and can deal with different numbers of variables in different events. However, its practical application requires the careful selection of variables with reduced correlations among them. The description of this likelihood ratio method, the set of variables used and the performance of the DELPHI combined b-tagging is given below.

4.1 Description of Method

The combined tagging variable y in the likelihood ratio method is defined as:

$$y = \frac{f^{bgd}(x_1, ..., x_n)}{f^{sig}(x_1, ..., x_n)} \tag{15}$$

where $f^{bgd}(x_1, ..., x_n)$, $f^{sig}(x_1, ..., x_n)$ are the probability density functions of the discriminating variables $x_1, ..., x_n$ for the background and the signal respectively. The selection of all events with $y < y_0$ gives the optimal tagging of the signal. It should be stressed that such tagging is absolutely the best for a given set $x_1, ..., x_n$ of variables.

In practical applications the determination and utilisation of multi-dimensional probability density functions is quite difficult for $n > 2$. The solution consists in a special selection of discriminating variables having reduced correlations among them. In the limit of independent variables[5], expression (15) becomes:

$$y = \prod_{i=1}^{n} \frac{f_i^{bgd}(x_i)}{f_i^{sig}(x_i)} = \prod_{i=1}^{n} y_i; \tag{16}$$

$$y_i = f_i^{bgd}(x_i)/f_i^{sig}(x_i) \tag{17}$$

[5]Two variables are independent if, for the signal and for each separately treated background component (e.g. c and uds), the distribution of one is independent of any selection on the other.

where $f_i^{bgd}(x_i)$, $f_i^{sig}(x_i)$ are probability density functions of each individual variable x_i for the background and signal, and are determined from simulation.

This scheme is used in DELPHI to construct the combined b-tagging. For each individual variable x_i the value y_i is computed from (17); the combined tag y is defined as the product of the y_i. It is not exactly optimal any more, because the discriminating variables are not independent, but the variables are chosen such that the correlations between them are small enough that the resulting tagging is very close to optimal. Furthermore, the efficiencies and mis-tag rates are determined from simulation (and sometimes from the actual data), thereby taking into account any small correlations.

In DELPHI all discriminating variables and the b-tagging itself are computed independently for each jet in an event, where ideally all tracks coming from the fragmentation of the b-quark and from the decay of the b-hadron are combined in one jet by a jet clustering algorithm. In this case the background for the b quark selection can be separated into two different parts – jets generated by c-quarks and by light ($q = u, d, s$) quarks. These two components are independent and have very different distributions of discriminating variables.

To define the extra discriminating variables for the b-tagging, tracks are selected so as to come preferentially from b-hadron decay. For this purpose all jets in an event are classified into 3 categories. In the first category all jets with one or more reconstructed secondary vertices are included. A reconstructed secondary vertex provides a clean selection of b-hadron decay products and a large number of discriminating variables can be defined in this case. If the secondary vertex is not reconstructed, tracks from the B decay are selected by requiring the track significance probability to be less than 0.05, and the second category includes all jets with at least 2 such offsets. This criterion is less strong, allowing more background jets to pass the cut. Finally, if the number of offsets is less than 2, the jet is included in the third category and in this case only a reduced set of inclusive discriminating variables, like the lifetime probability (see Section 3.5), is used. In Z hadronic events the fractions of jets classified into categories 1, 2, 3 are 44%, 14%, 42% respectively for b-quark, 8%, 8%, 84% for c-quark and 0.6%, 2.8%, 96.6% for light quark jets.

The tagging variable y_α for a jet of category α is defined as:

$$\begin{aligned} y_\alpha &= n_\alpha^c/n_\alpha^b \prod_i y_{i,\alpha}^c + n_\alpha^q/n_\alpha^b \prod_i y_{i,\alpha}^q; \qquad (18) \\ y_{i,\alpha}^{(c,q)} &= f_{i,\alpha}^{(c,q)}(x_i)/f_{i,\alpha}^b(x_i) \end{aligned}$$

where $f_{i,\alpha}^q(x_i)$, $f_{i,\alpha}^c(x_i)$, $f_{i,\alpha}^b(x_i)$ are the probability density functions of x_i in jet category α generated by uds, c and b quarks respectively and n_α^q, n_α^c and n_α^b are their normalised rates, such that $\sum n_\alpha^q = R_q$, $\sum n_\alpha^c = R_c$, and $\sum n_\alpha^b = R_b$. R_q, R_c and R_b are the normalised production rates of different flavours and $R_q + R_c + R_b = 1$.

As can be seen from eqn. (18), the classification into different categories effectively works as an additional discriminating variable with the discrete probabilities given by $n_\alpha^{(q,c,b)}$. For example, the b-purity of a sample of jets with reconstructed secondary vertices is about 85%. However, the primary purpose of this separation is to allow the use of a larger number of discriminating variables when a secondary vertex is found. The search for the secondary B decay vertex is thus an important ingredient of DELPHI b-tagging.

It is often convenient to define $X_{jet} = -\log_{10} y_\alpha$ as the jet tagging variable, and this variable is used in all applications described in Section 6. The event variable X_{ev} is defined as the sum of the largest two X_{jet} values for the individual jets in the event.

4.2 Secondary Vertex Reconstruction

A secondary vertex (SV) is searched for in each jet of the event. In the first stage all possible combinations of pairs of tracks are selected as SV candidates if they have a common vertex with the χ^2 of the fit less than 4. After that all tracks from the same jet are tested one by one for inclusion in a given SV candidate. The track producing the smallest change Δ of the vertex fit χ^2 is included in the SV candidate if this change does not exceed the threshold $\Delta = 5$. This value and all other numerical parameters of the algorithm were selected by optimising the efficiency of the SV reconstruction and background suppression. This procedure is repeated until all tracks satisfying the above condition are included in the SV candidate. The SV candidate is rejected if the distance to the primary vertex divided by its error is less than 4. Additionally, at least two tracks in the SV candidate are required to have VD measurements in both $R\phi$ and Rz planes.

The decay of the b-hadron is usually followed by decays of one or two D mesons, thereby producing several secondary vertices. It thus often happens that some secondary tracks cannot be fitted to a single secondary vertex. However, the spatial distance between any secondary track and the flight trajectory of the b-hadron should be small since the D-mesons tend to travel in the direction of the initial b-hadron. Using this property some tracks of far-decaying D mesons can be recuperated, which is important for the computation of such quantities as the b-hadron mass. The flight trajectory of the b-hadron is defined as the vector from the primary to the secondary vertex. Any track from the same jet having an $R\phi$ or Rz component track probability less than 0.03 and not included in the SV fit is attached to the SV candidate if its distance in space to the flight trajectory divided by its error is less than 3. Although not included in the SV fit, such tracks are used in the computation of all discriminating variables.

Sometimes the decay vertex of a D-meson can be reconstructed separately from the b-hadron decay vertex, which then results in two or more secondary vertices in the same jet. In that case, all tracks included in these vertices are combined for the computation of the b-tagging discriminating variables.

Three additional criteria are used to suppress the background of light quarks in the sample of jets with secondary vertices. The first one makes use of the momentum vector of the b-hadron. This is defined as the sum of the momenta of all tracks included in the SV candidate. Additionally, the momenta of all other neutral and charged particles with pseudo-rapidity exceeding 2 are also included; the pseudo-rapidity is computed with respect to the flight direction of the b-hadron. Then, the trajectory directed along the B-momentum and passing through the SV position is constructed and the impact parameter δ_{SV} of this trajectory with respect to the primary vertex is computed. For a real b-hadron the momentum direction should be close to the flight direction and δ_{SV} should be small compared to its error[6] $\sigma_{\delta_{SV}}$, while for a false secondary vertex the flight and momentum directions are much less correlated. Therefore SV candidates with $(\delta_{SV}/\sigma_{\delta_{SV}})^2 > 12$ are rejected. For the second criterion the lifetime probability using all tracks included in the SV candidate is computed and the candidate is rejected if this probability exceeds 0.01. The third criterion requires the distance between the primary and secondary vertex to be less than 2.5 cm, because the contribution of false secondary vertices and of strange particle decays becomes rather high at large distances. Any background jet with a very distant SV would give an extremely strong b-tagging value and this cut effectively rejects such cases.

[6] $\sigma_{\delta_{SV}}$ is computed using the uncertainties in the positions of primary and secondary vertices and the uncertainty in the B-hadron flight direction estimate, obtained from the simulation.

Candidates remaining after these selections are considered as reconstructed secondary vertices. With this procedure a SV is reconstructed for about 44% of jets with b-hadrons (50% for jets inside the VD acceptance). The b-purity of the sample of jets with a reconstructed SV is about 85% for hadronic decays of the Z, which should be compared with the initial b-purity of about 22%. More than one SV in a single jet is allowed, reflecting the possibility of cascade ($B \to D$) decays giving rise to distinguishable secondary vertices. In this case the tracks from all secondary vertices are combined for the computation of the SV discriminating variables.

4.3 Discriminating Variables

In this section the discriminating variables used in b-tagging are described. All definitions are given first for jets with reconstructed secondary vertices. Then the modifications for other jet categories are described. All discriminating variables, except the transverse momentum of a lepton, are computed using the charged particles included in the secondary vertex.

The jet lifetime probability, P_j^+, is constructed using equation (14) from the positive IPs of all tracks included in the jet.

The mass of particles[7] *combined at the secondary vertex*, M_s, is very sensitive to the quark flavour. The mass at the secondary vertex in a jet generated by a c-quark is limited by the mass of the D-meson, which is about 1.8 GeV/c^2, while the mass in a b-jet can go up to 5 GeV/c^2. The limit of 1.8 GeV/c^2 for the c-jets can be clearly seen in fig. 14(a). Some c-jets do have a higher value of M_s due to tracks incorrectly attached to the SV.

The fraction of the charged jet energy included in the secondary vertex, X_s^{ch}, reflects the differences in the fragmentation properties of different flavours. The fragmentation function for the c-quark is softer than for the b-quark, as seen in the distribution of X_s^{ch} in fig. 14(b).

The transverse momentum at the secondary vertex, P_s^t, first introduced by the SLD collaboration [12], takes into account missing particles not included in the SV definition. P_s^t is defined as the resultant transverse momentum (with respect to the b-hadron's estimated flight direction) of all charged particles attached to the SV. Missing particles can be neutrinos from semileptonic decay, other neutral particles or non-reconstructed charged particles. In all cases, due to the high mass of the b-hadron, the value of P_s^t for b-quark jets is higher, as can be seen from fig. 14(c).

The rapidity of each track included in the secondary vertex, R_s^{tr}, is quite a strong discriminating variable, significantly improving the b-quark selection. Although a b-hadron on average is produced with a higher energy, the rapidities of particles from B-decays are less than those from D-meson decay, as can be seen from fig. 14(d). This is mainly explained by the higher b-hadron mass. The variable R_s^{tr} is defined for each track in the SV and the corresponding variable y_R for each track is used in (18) for the computation of the b-tag. Although there is overlap between the signal and background for an individual track rapidity, because of the large number of secondary tracks the inclusion of all the rapidities in the b-tag results in a significant gain.

The transverse momentum of an identified energetic lepton, p_l^t. It is independent of the track IP and can be defined for any category of jet containing a muon or electron. A more detailed description of this variable and of some specific features of its inclusion in the combined b-tagging scheme are given in the next section.

[7] For computation of discriminating variables, such as mass or track rapidity, elsewhere in this paper, charged particles are given the pion mass, whereas neutrals (except for K_s^0 and Λ) are assumed to be massless.

All these variables are defined for the first category of jets (with reconstructed SV). For the two other categories, a reduced set of variables is used. For jets with at least two offsets, the jet lifetime probability, the effective mass of all tracks with offsets, their rapidities and any lepton transverse momentum are computed. For jets with less than two offsets the effective mass is not used, as there is no reliable criterion for selecting the particles from B-decay; however the track rapidities for all tracks with positive IP are still included in the tagging. The ratios of probability density functions are computed separately for each jet category. The possibility of treating in the same way different categories of events with different sets of discriminating variables is a very important feature of the likelihood ratio method of b-tagging.

The distributions of M_s, X_s^{ch}, P_s^t and R_s^{tr} are shown in figure 14. These distributions are shown for b-quark jets and also for c-quark jets, the latter constituting the main background for b-tagging.

Combined b-tagging using the complete set of discriminating variables performs much better than the simple lifetime tagging. This is illustrated in fig. 15. The performance is tested using jets of Z hadronic decays. The figure shows the contamination of the selected sample by other flavours ($N_{udsc}/(N_{udsc}+N_b)$) versus the efficiency of b-jet selection. Compared with the tagging using only P_j^+, combined tagging provides much better suppression of background, especially in the region of high purity. A very pure sample with contamination below 0.5% can be obtained for a sizable b efficiency, which opens new possibilities for measurements with b-hadrons.

4.4 Lepton Tagging

Leptons with high transverse momentum have long been used in a variety of ways to identify the quark flavour of the jet from which they originate. This section describes the inclusion of this information within the standard DELPHI b-tagging algorithm.

Knowing the probabilities $P^{q,c,b}$ of finding a lepton in a light quark-jet, a c-jet or a b-jet respectively, and the transverse momentum distributions $f^{q,c,b}(p_l^t)$ of these leptons, the contribution of identified leptons to the global discriminating variable (18) is:

$$y_{p_l^t}^{(c,q)} = \begin{cases} \frac{f^{(c,q)}(p_l^t)}{f^b(p_l^t)} \frac{P^{(c,q)}}{P^b} & \text{if a lepton is found,} \\ \\ \frac{1-P^{(c,q)}}{1-P^b} & \text{otherwise,} \end{cases} \tag{19}$$

The quantities appearing in this expression are extracted from a sample of simulated hadronic Z decays, where all reconstructed particles are clustered into jets.

Reconstructed particles are identified as leptons if they satisfy a tight electron tag (from energy loss by ionisation in the TPC, or from associated energy deposits in the electro-magnetic calorimeters), a tight muon tag (from the muon chambers only), or a standard muon tag confirmed by a minimum ionisation energy deposit in the hadron calorimeters. Detailed descriptions of these different categories of tags and of their performance are given in ref. [7]. The quantities $P^{q,c,b}$ are simply defined as the fractions of jets of the corresponding flavour inside which a lepton is identified, and are 3%, 9.8% and 18.7% for light quarks, c-quarks and b-quarks respectively.

The transverse momentum of the lepton is evaluated with respect to the jet to which it belongs, when the lepton momentum is subtracted from the total jet momentum. The tagging contribution $y_{p_l^t}^{(c,q)}$ of the leptons is then obtained from the ratio of the transverse momentum distributions $f^{(c,q)}(p_l^t)$ and $f^b(p_l^t)$.

Figure 16 shows the superimposed distributions of transverse momenta for leptons found in b-jets, c-jets, and light quark-jets. The agreement of these with the data obtained from real hadronic Z decays (recorded in 1994) is excellent. Because of the small branching ratio of b-hadrons to high p_l^t leptons, the intrinsic discriminating power of lepton tagging is weaker than that of lifetime and secondary vertex information. However, it does provide useful information since it is fully independent of the above, and supplements the b-tagging in particular when no other hints of B decays are found (for example in case of fast decay, or decay outside the vertex-detector acceptance).

In principle, the distribution in transverse momentum at the secondary vertex P_s^t depends on whether or not there is a lepton present, because it is accompanied by an unseen neutrino. However, because semi-leptonic decays are multi-body, there is not a strong correlation between the lepton and the neutrino transverse momenta, and the difference in the P_s^t spectra (i.e. with and without charged leptons) is small, as can be seen from fig. 17.

The use of the algorithm at LEP2 requires some additional care. In this case, data available for detector calibration are less abundant, and some experimental aspects are less well understood. In particular, lepton identification or misidentification probabilities are not perfectly reproduced, and this leads in general to an excess of simulated events with respect to real data, mainly in the low transverse momentum region. To correct for this, rejection factors are computed for each category of identified leptons in the simulation, and applied randomly.

Finally, it is not obvious that lepton tagging calibrated on Z data will produce efficient discrimination in the context of Higgs searches at LEP2, especially in 4-jet events. This is because in the Higgs search events are reconstructed by constraining the number of jets rather than fixing the jet algorithm resolution parameter as was done for the calibration; as a result the measured transverse momentum distributions are different. Figure 18 shows the distributions of the flavour ratios (*i.e.* the discriminating power) after the applied corrections. The data at the Z and at high energy are in fact in approximate agreement.

4.5 Event b-tagging

b-hadrons are almost always produced in pairs and the presence of the second b-hadron significantly improves the b-tagging of an event as a whole. The likelihood ratio method provides a simple way for combining the information from the two b-hadrons. Keeping in mind that each flavour is produced independently from all other flavours, one can write the equation for the event tagging variable, where the two jets[8] are of categories α and β, as:

$$y_{\alpha\beta}^{ev} = \frac{R_b}{R_c}\frac{n_\alpha^c n_\beta^c}{n_\alpha^b n_\beta^b}\prod_i y_{i,\alpha}^c \prod_i y_{i\beta}^c + \frac{R_b}{R_q}\frac{n_\alpha^q n_\beta^q}{n_\alpha^b n_\beta^b}\prod_i y_{i,\alpha}^q \prod_i y_{i\beta}^q \tag{20}$$

It was found, however, that a simpler way of combining the information from two jets into a single tagging variable:

$$y_{\alpha\beta}^{ev} = y_\alpha \cdot y_\beta \tag{21}$$

works equally well. Here y_α, y_β are given by eqn. (18). The difference between these two equations is that (21) neglects the correlated production of the same background flavours in an event. The b-tagging variable computed from (21) was used in the Higgs search (see Section 6.5).

[8] In events with more than 2 jets, the smallest two values of y were used.

Figure 15 compares the performance of event tagging and of jet tagging for Z events. As can be seen, very strong suppression of background (down to 10^{-3} level) can be achieved with event tagging.

4.6 Equalised Tagging

Physics analyses at the edge of detector capabilities, like the search for a Higgs boson, demand extremely high performance of the b-tagging. The only way to achieve this objective is to expand the set of discriminating variables. But adding a new variable in the combining relation (16) becomes more and more difficult with the growth of their number due to the increasing influence of correlations among them.

However, the combined method can be modified to include correlated variables. The main idea of the combined method which guarantees optimal tagging for non-correlated variables consists in assigning the same value of the tagging variable to different events having the same likelihood ratio for background to signal. As described below, the consistent application of this principle while extending the set of discriminating variables gives a desirable improvement of the tagging performance. The simplest way to explain this approach is to consider a particular example, obtained from simulation samples and presented in figure 19.

The upper plot in fig. 19 shows the simulated distributions of charged multiplicity N_{ch} in b-jets from the process $e^+e^- \to HZ$ and in light quark jets from $e^+e^- \to W^+W^-$. The latter process presents the main background for the SM Higgs search, and is suppressed mainly by the b-tagging. The fact that these two distributions are different implies that it is useful to include this variable in the tagging. The lower plot in fig. 19 shows the ratio $R(W^+W^-/HZ)$ of the number of light quark jets from the $e^+e^- \to W^+W^-$ process to that of b-jets from $e^+e^- \to HZ$ in the simulation, as a function of the tagging variable X_{jet}:

$$X_{jet} = -\log_{10} y_{jet}, \tag{22}$$

where y_{jet} is defined by equations (16-17). Two subsamples of events with $N_{ch} < 7$ and $N_{ch} > 19$ are considered separately. As can be clearly seen, for the same value of X_{jet} the ratio $R(W^+W^-/HZ)$ in the two subsamples is different. Events with the same value X_{jet} are thus not equivalent; in one subsample they will contain more background contamination than in the other. To restore their equivalence, the variable X_{jet} should be modified in such a way that all events with the same value of X'_{jet} in different subsamples will have the same ratio $R(W^+W^-/HZ)$. Due to the equivalence principle formulated above, such a modification should give better tagging. Technically, *equalising* of X_{jet} is achieved by a linear transformation:

$$X'_{jet} = A \cdot X_{jet} + B, \tag{23}$$

assuming that the dependence of $R(W^+W^-/HZ)$ on X_{jet} in each case can be approximated by an exponential, as shown in fig. 19. The coefficients A and B are different for each subsample; their calculation using the parameters of the exponential functions is straightforward.

Including a new independent variable x_{new} in the tagging using (16) is equivalent to the transformation $X'_{jet} = X_{jet} - \log_{10} y_{new}$, where $y_{new} = f^{bgd}(x_{new})/f^{sig}(x_{new})$, i.e. it is a particular case of (23). Such a simple transformation cannot be used for N_{ch} because of its strong correlation with other discriminating variables, which is reflected in the

significantly different slopes of the lines in fig. 19. Instead, the transformation (23) works reasonably well.

A practical application of the equalising method is to the Standard Model Higgs boson search. A set of additional discriminating variables is defined for each jet of the event. For each new variable, jets are classified in 3 to 5 subsamples. For example, for N_{ch} these subsamples are: $N_{ch} < 7$; $7 \leq N_{ch} < 12$; $12 \leq N_{ch} < 20$; $N_{ch} \geq 20$. For each subsample the transformation (23) is applied independently and the new tagging variable X'_{jet} is computed. The parameters of the transformation are determined from the condition that the dependence of $R(W^+W^-/HZ)$ on the modified X'_{jet} becomes the same for all subsamples. The variables are included in the tagging sequentially. For each new variable, the X'_{jet} obtained at the previous step is used. As before, the global event b-tagging variable X_{evt} is defined as the sum of the two highest X'_{jet} values among all jets in the event.

The additional variables included in the b-tagging using this equalising method reflect mainly kinematic properties of b-quarks. They are: the polar angle of the jet direction; the jet energy and invariant mass; the charged multiplicity of the jet; the angle to the nearest jet direction; and the number of particles with negative IP.

Returning to the example of N_{ch}, fig. 20 shows that equalising over this variable improves the suppression of the $e^+e^- \to W^+W^-$ background. As can be seen from fig. 19, the largest difference between subsamples with different N_{ch} is observed at low X_{jet} values, while the background suppression at high X_{jet} is almost the same. The main improvement from the equalising procedure can thus be expected for the low purity / high efficiency tagging, corresponding to low X_{jet} values. Exactly such behaviour is observed in fig. 20: including N_{ch} gives almost no improvement for the region of strong background suppression. However, equalising the b-tagging for the complete set of variables given above suppresses the $e^+e^- \to W^+W^-$ background by an extra factor of more than 2 over a wide range of $e^+e^- \to HZ$ efficiency. This additional suppression is important for the Higgs boson search since it results in a sizable increase of its detection sensitivity.

The same equalisation procedure was applied for the $e^+e^- \to hA$ channel when both Higgs bosons decay into $b\bar{b}$, which is the dominant channel with BR larger than 90% at LEP2 energies. A new X^{hA}_{jet} was constructed with the condition that all events with the same value of X^{hA}_{jet} in different subsamples will have the same ratio $R(W^+W^-/hA)$. The X^{hA}_{jet} variable was used in the search of the hA 4b channel as described in section 6.5.

4.7 Different Ways of Combining Variables

As can thus be seen, for combining the separate variables that are relevant for b-tagging, three different methods have been used :

- The IPs of the different tracks are combined by constructing the lifetime probability P^+ from the probabilities for the significance values of the various tracks (see Section 3.5);
- For the different variables contributing to the 'combined tag', a likelihood ratio method is used, as described in Section 4.1;
- For extra variables, the 'equalisation' method of Section 4.6 is used.

To some extent these differences are a result of the historical evolution of our b-tagging algorithms, but there is some underlying logic to these differences. Thus the likelihood ratio method is guaranteed to give the optimal signal/background ratio even for correlated variables (assuming of course that the simulation accurately describes the data,

including the correlations). However, the method is much simpler when the variables are uncorrelated, and this is how the likelihood ratio method was used in 'combined tagging'.

This could have been used for combining the individual IPs, since the error correlations between tracks are small. However, it would have been necessary to produce signal/background probability ratios separately for each class of track (i.e. for each pattern of hits in the VD). We preferred to use the lifetime probability, where instead the tuning was performed separately for the different track classes.

Finally, for the Higgs search, extra variables were included to improve the b-tagging performance. Some of these had significant correlations with those already used, so they could not simply be added as extra variables in an extended combined tagging approach. This led instead to the 'equalised tagging'.

5 Modelling and Tuning of Mass-related Parameters

The agreement between data and simulation is sensitive to the modelling of the physics in the event generator, and to the tuning of its parameters. A detailed description of the physics model in the main generator used by DELPHI at LEP can be found in [16]. The strategy adopted for the parameter tuning and its corresponding results can be found in [17]. In this section, two aspects of the modelling are mentioned, which are specially relevant in the context of b-tagging, and which have been investigated recently [18, 19]: the modelling of the rate of gluons radiated off b-quarks relative to light quarks, and the probability of secondary b-quark production through gluon splitting. Both quantities affect the description of the dependence of R_b on the jet multiplicity (and on event shape variables), and depend critically on the way quark mass parameters are introduced in the treatment of the quark fragmentation and subsequent hadronization used in the generator. They are important for several of the measurements in Section 6, particularly those involving the analysis of multi-jet b-tagged events, such as the measurement performed at LEP1 of the running b quark mass at the M_Z energy scale (see Section 6.4), and the LEP2 Higgs boson search (see Section 6.5).

5.1 Treatment of Gluon Radiation off b-quarks

Discrepancies between simulation and data were observed, which could be attributed, entirely or at least partly, to imperfect modelling of mass effects in the generator. As an example, the R_b fraction evaluated separately for two and three jet events, using the method described in Section 6.1, is illustrated in figs. 21, where JETSET version 7.4 [16] was used for the simulation. Similar behaviour is observed in the comparison of two and four jet events.

Because of their higher mass, b-quarks radiate fewer gluons than lighter flavours. This results in fewer multi-jet events in the case of b-quarks. From kinematic arguments, the suppression scales approximately as $m_b^2/(s \cdot y)$, where m_b, s and y are the b mass, the square of the collision energy and the jet resolution parameter, respectively [20]. It is observed explicitly in the value of R_3^{bq}, the double ratio of the 3-jet rate for b and light quarks,[9] used in the measurement of the running b-quark mass at the M_Z energy scale (see Section 6.4). Quantitatively the suppression is of order 5%.

In the original JETSET prescription, used up to version 7.3, mass effects were ignored altogether, both in the parton shower evolution describing the fragmentation of the quarks,

[9] R_3^{bq} is defined as the ratio of the b-quark and light quark rates in 3-jet events, divided by the corresponding flavour ratio for events with any number of jets

and in the 3-parton matrix element used to correct the first emissions of quarks and anti-quarks in the shower. The phase space treatment did include masses, however, and induced a large suppression of radiation from the b quark. In version 7.4, and later in PYTHIA versions up to 6.130, an intermediate "improvement" was introduced, in that matrix element expressions incorporating quark masses were now used in the matching procedure. The suppression of the radiation resulting from this intermediate treatment, which was in place during much of the LEP period, was however exaggerated by as much as a factor of 2, and resulted in the largest discrepancy with the data [18, 19]. Starting with PYTHIA version 6.130, and up to version 6.152, mass effects were also introduced in the shower evolution through a correction to the expressions of the probabilities of the first branchings of each quark. From PYTHIA version 6.153, a fully consistent treatment is available, including a massive treatment of all branchings in the shower, now taking into account in the specification of the matrix element the nature of the couplings of the source (vector, axial,...) decaying into quarks, as well as the possibility of unequal quark masses (as in the case of $W \to c\bar{s}$). Considerable overall improvement was achieved in the description of both b-tagged 3– and 4–jet rates, thanks to these developments [18,19].

5.2 Treatment of Gluon Splitting to b-quark Pairs

Secondary b-quark pair production from gluon splitting can also result in b-tagged multi-jet events. The corresponding rate is small but is poorly known both theoretically and experimentally. This implies an uncertainty in the predictions, particularly of the b-tagged 4-jet rate at LEP2 energies.

Measurements by LEP and SLD collaborations at $\sqrt{s} = M_Z$ give $g_{b\bar{b}} = (0.254 \pm 0.051)\%$ [21], where $g_{b\bar{b}}$ is defined as the fraction of hadronic events containing a gluon splitting to a $b\bar{b}$ pair. This is consistent with the best theoretical estimates, which are around 0.2% [18], with relative uncertainties due to unknown sub-leading logarithmic corrections, which may be as large as 30%.

The rate predicted by Monte Carlo generators based on parton shower methods is also sensitive to the treatment of sub-leading and kinematic effects in the shower evolution. While the original JETSET and PYTHIA prescription resulted in only 0.15%, since version 6.131 a set of new options has been introduced which bring this rate closer to the measured values [18]. Two of these options, which almost exactly double the original rate, have been recommended [18] and are used in the latest simulations at LEP2 energies[10]. The first of these options (MSTJ(44)=3) uses the mass of the virtual gluon involved in a splitting to define the scale $m_g^2/4$ relevant for α_s, the strong coupling constant, rather than the default p_T^2 prescription used for other types of branchings in the shower evolution. The second option (MSTJ(42)=3) reduces the conditions on coherence in the emissions, in the case of gluon splittings into heavy quark pairs, by introducing a mass correction into the angular criterion used to restrict the successive branchings in the shower.

The impact on the b-tagged 4-jet rate at LEP2 is best illustrated in the context of the Higgs search or of the measurement of Z boson pair production. At LEP2 energies the rate of gluons which can split into b quark pairs is less suppressed by kinematics than at LEP1. For instance at 189 GeV it is as large as 0.4% using the original JETSET and PYTHIA prescription. In a subsample of events enriched with 4-jet events, it can reach levels near 1% depending on the criterion used on the jet resolution parameter. With the new options described above, these values are roughly doubled. The effect of this doubling on the Higgs search was studied by comparing the numbers of events predicted

[10] For simulations performed with versions of PYTHIA prior to 6.131, a re-weighting procedure was used to increase the $g \to b\bar{b}$ rate by a factor of about 2.

to be selected, when assuming the default value for the rate of gluon splittings into b quark pairs or the doubled one. The relative difference between these two numbers is about 2.5%; it varies slightly with the b-tagging cut but does not exceed 5%. It was taken into account in the final evaluation in this channel (see Section 6.5 and references therein).

6 Physics Applications

In this section, some analyses involving b-tagging are described. The aim is not to present the physics results, which have already been published, but rather to illustrate how b-tagging works in practice. The extent to which uncertainties in tagging influence the final results is also mentioned. Much more detail, including the estimation of systematics, can be found in the published papers.

6.1 Measurement of R_b at the Z

One of the most challenging measurements at LEP1 is the determination of R_b, the branching ratio for Z hadronic decays into b-quarks. All accurate measurements of R_b use the so-called double tag method. This compares the fractions of events in which there is a b-tag in a single hemisphere with those in which both hemispheres are tagged. It allows the extraction from the data of both R_b and the efficiency ϵ_b for tagging a hemisphere as coming from a b-quark. We thus do not have to rely on the simulation for the calculation of this important quantity. The small background mis-tag rates, ϵ_c and ϵ_{uds}, and the correlation between hemispheres, ρ_b, are taken from the simulation. The tracks are separated into two hemispheres by the plane perpendicular to the thrust axis. The highest b-tagging value $X_{jet} = -\log_{10} y_{jet}$ (see eqn. (18)) of any jet in the given hemisphere is taken as the hemisphere tag.

The correlation ρ_b allows for the fact that there are small differences between the overall hemisphere b-tagging efficiency, and the efficiency for tagging a hemisphere if the other one has already been tagged. These correlations arise, for example, from the fact that at the Z, hadronic events tend to consist of back-to-back jets; if one jet is at large positive cosθ where the tagging efficiency is lower (see fig. 3), then the other jet is likely to be at large negative cosθ, again with lower efficiency; thus the efficiencies are correlated. The systematic uncertainty on ρ_b was estimated by comparing data and simulation for various kinematic variables that were sensitive to the separate contributions to ρ_b.

In particular, it was found that a large correlation arose from the use of a common PV for the whole event; if the PV was badly measured as being closer to the SV in one hemisphere, then the IP values in that hemisphere would all be systematically reduced in magnitude, while those in the opposite hemisphere would be increased. This was overcome by determining a separate PV for each hemisphere of the event. This modification slightly reduced the flavour discrimination power of the algorithm, and hence increased the statistical error, in exchange for a large decrease in the correlation and a smaller systematic error.

Achieving high accuracy for R_b requires the following:

- the b-tag must reach very high efficiency to reduce the statistical error: $\delta R_b \sim 1/\epsilon_b$;
- at the same time the b-tag must have high purity to reduce the systematic errors coming from our knowledge of the background: $\delta R_b \sim \epsilon_x R_x/\epsilon_b$, where $x = q$ or c;

- there must be excellent agreement between data and simulation to reduce the systematic errors due to the modelling of the detector resolution, and because there are quantities taken from the simulation and not measured directly in the data.

In the DELPHI R_b measurement, both the crucial high-purity b-tag in the "multivariate" analysis [14], which finally gave the best precision, and the "combined b-tag" analysis used the combined hemisphere tag described earlier (see Section 4). This required the presence of a SV and included the hemisphere lifetime probability P_j, the SV mass M_s, the charged energy fraction X_s^{ch}, and the rapidities of the tracks at the SV. The missing transverse momentum P_s^t and the lepton transverse momentum P_l^t were not used.

The sources of the systematic error are our knowledge of b-hadron, charm- and light-quark physics (such as lifetimes, decay modes and multiplicities) and our understanding of the detector resolution. The first contribution is minimised by measuring the b-efficiency from the data itself and by reducing the charm- and light-quark mis-tag rates to the minimum possible so as to give a very pure b-tag. The second contribution is minimised by having good agreement between data and simulation for the detector resolution.

The high statistical precision of the result is mainly due to the high performance of the DELPHI b-tag: at 98.5% hemisphere b-purity, the hemisphere b-efficiency is 29.6%, while the mis-tag efficiencies $\epsilon_c = 0.4\%$ and $\epsilon_{uds} = 0.05\%$.

The smallness of the systematic error comes specifically from the fact that the contribution from the detector resolution understanding is very small. First, the DELPHI vertex detector has three layers of silicon detectors allowing better pattern recognition than for a detector with only two layers. The design of the detector is such that the intrinsic IP resolutions in both the $R\phi$ and Rz components are good – 27 and 39 μm respectively – and consequently also the precision of the primary and secondary vertex positions (see Sections 3.2 and 4.2). Secondly, the detector IP resolution is tuned with high accuracy, as described in section 3.6, resulting in a good agreement between data and simulation (see fig. 13(b)). As a consequence the error coming from our understanding of the detector resolution amounts to only 20% of the total error.

In summary the performance of the b-tag and the understanding of the detector resolution result in very good stability of the R_b measurement as a function of the b-efficiency as shown in fig. 22; the highest and lowest efficiencies shown of 44.0% and 21.0% correspond to b-purities of 91.6% and 99.4% respectively. Thus, a stable R_b result was obtained while the background contribution varied by more than a factor of 10. The total relative error was only 0.4%.

6.2 R_{4b}, the Rate of Events with 4 b-quarks at the Z

Four b jets are produced predominantly when, in an event with a b pair, a gluon is radiated from one of the quarks and itself produces another b pair. This analysis thus gives information on the $gb\bar{b}$ coupling.

The high purity and efficiency of the tagging method, together with the good agreement between data and simulation, allowed DELPHI to measure for the first time the rate of Z events with 4 b-quarks in the final state [22]. R_{4b} has been measured to be (6.0 $\pm$ 1.9 (*stat*) $\pm$ 1.4 (*syst*)) $\times$ 10^{-4} at a signal efficiency ϵ_{4b}=(3.16$\pm$ 0.11)%. The analysis required 3 jets identified as coming from b-quarks. This means that the b-efficiency enters to the third power, demanding a very high efficiency of a tight b-tag. The high purity of the tag is required in order to suppress the background from gluon splitting into c-quarks, that is a factor of 10 higher than the splitting into b-quarks. Thus, the measurement relies on the b-tagging performance and data/MC agreement in the b-tagging of the third

jet, sorted by decreasing b-tag value, see fig. 23. The uncertainty coming from the b-tag amounts to only 6% of the total systematic error and is determined mainly by the IP resolution description.

This analysis used the b-tag algorithm of Section 6.1, except that if no SV was found, the jet lifetime probability P_j was used by itself.

6.3 Measurement of the b-hadron Charged Multiplicity

The good agreement between data and simulation achieved by the tuning of the track resolution allowed DELPHI to measure with very high precision the charged multiplicity n_B of weakly decaying b-hadrons [23]. The basis for the measurement is the determination of the number of tracks in a b-jet which come from the SV rather than from the PV. In the hemisphere opposite to the b-tagged one, the difference

$$N_{+-} = n^+ - n^- \tag{24}$$

is computed, in which n^+ and n^- are the numbers of tracks with positive and with negative IP respectively. The quantity N_{+-} is obtained as a function of the b-tagging purity and the value of n_B is extracted by comparing N_{+-} from data and simulation, extrapolated to the limit of 100% b-purity.

The result was $n_B = 4.97 \pm 0.03 \pm 0.06$. The measurement reaches 1.3% precision, due to the good understanding of the IP resolution, to the efficient method for determining the sign of the IP (see Section 3.3) and to the precision of the VD alignment (see section 2.2). The tracking efficiency is 99±1%(syst), its uncertainty dominates the systematic error on n_B.

This analysis used the same b-tag algorithm as the previous analysis.

6.4 Measurement of the Running b-quark Mass at M_Z

The b quark mass determination at the M_Z scale has been performed by DELPHI by measuring the R_3^{bq} observable, as defined in Section 5.1. Two different jet-finding algorithms, DURHAM [24] and CAMBRIDGE [25], were used to reconstruct the jets. Special features of this analysis in connection with the flavour tagging performance of DELPHI are:

- b and q initiated events are selected using the same technique,
- the efficiency versus purity working points are chosen so as to minimise the total error on the result (including effects from corrections and biases).

The directly measured observable, $R_3^{bq-meas}$, had to be corrected for detector acceptance effects, for kinematic biases introduced by the tagging procedure and for the hadronization process in order to get the observable at the parton level, R_3^{bq-par} [26]. This quantity was then compared with theoretical predictions based on 'Next to Leading Order' analytic calculations [20] to evaluate the b-quark mass at the M_Z energy scale.

In the original analysis [26], q- and b-quark initiated events were selected by the lifetime-signed IPs of charged particles in the event (see Section 3.5). In more recent versions of the analysis, the combined tagging technique of Section 4 has also been used. The flavour composition of the samples tagged as q-quark and as b-quark by the two methods are shown in Table 1.

The magnitude of the corrections applied in each of the two b-tagging techniques is illustrated in fig. 24, where the corresponding $R_3^{bq-meas}$ observables are shown, using

Method	Tagged Sample	Actually q (%)	Actually c (%)	Actually b (%)
IP	q	85.8	12.6	1.7
IP	b	5.0	15.3	79.7
Comb	q	82.0	15.5	2.5
Comb	b	4.3	10.4	85.4

Table 1: Flavour compositions of the samples tagged as q-quark and b-quark events for each tagging method.

simulated DELPHI data and the DURHAM jet finding algorithm, together with the parton-level one, R_3^{bq-par}, obtained with `PYTHIA` 6.131. For $y_c = 0.02$, the corrections are 10% for both techniques, although in opposite directions.

For the simulation the same corrected result is (obviously) obtained, but for real data this is not the case. This difference between the two techniques arises mainly from the imperfect modelling of the physics processes affecting the fragmentation and decay of heavy and light quarks. Half of this difference is taken as the systematic uncertainty associated with this measurement. The error induced by the tagging uncertainties is in the range 0.3% to 0.4%, compared with the total error of order 1% on the flavour independence of the strong coupling constant. In terms of the running b-quark mass, these errors correspond to 150 and 500 MeV respectively.

6.5 Higgs Searches in 4-jet Topology

One of the main topics at LEP2 energies has been the search for the SM Higgs boson, both in the Standard Model (SM) and in the Minimal Super-Symmetric Model (MSSM). Here the approach used in the dominant 4-jet channel is outlined.

Radiative production from a virtual Z $e^+e^- \to Z^* \to HZ$ is (in principle!) the main Higgs process at LEP2 and is referred to as Higgsstrahlung. The mass of the Higgs boson is at present unknown, but for a given mass its other properties are determined from the SM. The Higgs boson couples to massive fermions and to the $W^\pm$ and Z bosons.

The predominant decay mode for the SM Higgs in the mass range of interest for LEP2 searches is expected to be to pairs of b quarks with a branching ratio ranging from 87% to 80% with increasing Higgs mass. The same decay modes are dominant for h and A for many choices of values of the parameters in the MSSM, in particular for $\tan\beta > 1$. The identification of b jets and rejection of non-b jets is the most important ingredient in the majority of analyses designed to search for the neutral Higgs boson.

The four-jet final state includes the Higgs boson decaying to $b\bar{b}$, and also in principle to $q\bar{q}$ or gg. It is characterised by a large amount of visible energy. As the Higgs boson decays mainly to b quarks, when the Z also decays to $b\bar{b}$ the event will contain 4 b jets. If instead the Z decays to other quark pairs, the topology will again be 4 jets, but with only two of them due to b's.

The main backgrounds are two-fermion processes $e^+e^- \to q\bar{q}(\gamma)$, and four fermion processes involving W^+W^- and ZZ. Pair production of $W^\pm$ can result in c jets, but only very rarely in b jets. The ZZ is an irreducible background if the masses of the Higgs boson and of the Z are close, and the Z decays to $b\bar{b}$. The cross-sections of the

background processes are much higher than that for the Higgs production. At the highest LEP2 energies (around 208 GeV) and for $m_H = 114$ GeV/c^2, $\sigma_{Hqq} = 0.072$ pb while $\sigma_{4f} = 19$ pb and $\sigma_{2f} = 78$ pb.

In searches for the Higgs bosons at LEP2 in DELPHI, the various differences between b jets and light quark jets were accumulated in a single variable X_{jet} defined for each jet, as described in Section 4. Extra variables which help discriminate between the signal and background were included in the construction of the equalised tag (see Section 4.6). Including these extra variables in the tagging algorithm significantly improves the rejection of the light quark background.

The b-tagging value X_{ev} of the event in the search for the SM Higgs boson is defined as the maximum b-tagging value for any di-jet in the event, computed as the sum of the corresponding jet b-tagging values. In figure 25 the distribution of this equalised b-tagging variable is shown after the common four jet preselection [27] where good agreement between data and background simulation can be observed.

In the top part of figure 26 the performance of combined and equalised methods are compared for a SM Higgs boson mass of 114 GeV/c^2. As an example using only the b-tagging variable, for a signal efficiency of 40% the $q\bar{q}(\gamma)$ contribution is reduced to 5.6% using combined b-tagging, wheras it is even more strongly suppressed to 4.3% using equalised b-tagging. The WW component is reduced twice as much using equalised as compared with combined b-tagging.

In the bottom part of figure 26, the performance of the hA equalised b-tagging is shown in the $hA \to 4b$ channel and compared with the performance of combined b-tagging. The presence of four b-jets in the signal makes the analysis of the $hA \to 4b$ channel different from the HZ case, where in most of the cases only two b-jets are present. The event b-tagging value X_{ev}^{hA} for the Higgs boson search in the $hA \to 4b$ channel is defined as the minimum b-tagging value for any di-jet in the event and is computed as the sum of the corresponding jet b-tagging values. As can be seen, the application of the hA equalised b-tagging improves significantly the performance of the $hA \to 4b$ channel selection.

As an example using only the X_{ev}^{hA} b-tagging variable, for a signal efficiency of 50% the $q\bar{q}(\gamma)$ mistag rate is 0.8% using combined b-tagging, while it is reduced to 0.5% using equalised b-tagging. The WW efficiency is reduced from 0.1% to 0.06% when changing from combined to equalised tagging. The ZZ efficiency is also reduced from 3.7% to 3.3%.

In the search for the SM Higgs boson in the four jet channel, the b-tagging variable was combined with another set of discriminant variables [27] using an artificial neural network. The final confidence level estimation is calculated using two-dimensional information, where one dimension is the neural network output and the other is the reconstructed Higgs boson mass.

b-tagging is also used in the selection of the Higgs di-jet [27] from among the 6 possible Higgs di-jet candidates in a 4-jet event. The proportion of correct matchings for the Higgs di-jet, estimated in simulated signal events with 114 GeV/c^2 mass, is around 53% at pre-selection level, increasing to above 70% after the tight selection cut (see table 1 of [27]), while keeping a low rate of wrong pairings for ZZ background events.

7 Conclusion

The standard approach used by DELPHI for tagging b-hadrons has been described. By using not only the track impact parameters, which are sensitive to the longer lifetimes of hadrons containing b-quarks, but also other kinematic information related to secondary

vertices, track rapidities and any leptons, the efficiency/purity has been improved. For Z events, a purity of 98.5% for b-jets was achieved for an efficiency of 30%. Such high purity was required for the accurate measurement of R_b at the Z.

The tagging algorithm can also be applied to complete events, rather than just to single hemispheres. For the SM Higgs search at LEP2, the sum of the two largest b-tag variables for jets in the event was used. High efficiency b-tagging was required in order to extract any possible $H \to b\bar{b}$ decays from the large backgrounds. For a signal efficiency of 60%, a rejection factor of 140 for the W^+W^- background was achieved.

In contrast, the algorithm could be used in an anti-tagging mode, to select jets from light-quarks. This was used (together with conventional b-tagging), to compare the 3-jet rates for b- and for light quarks. This is sensitive to the b-quark mass.

For these and for other physics processes, it was crucial to have an efficient, well understood procedure for tagging b quarks. This resulted in systematic errors being kept to a minimum, and enabled many significant measurements to be performed.

Acknowledgements

We are greatly indebted to our technical collaborators, to the members of the CERN-SL Division for the excellent performance of the LEP collider, and to the funding agencies for their

support in building and operating the DELPHI detector.
We acknowledge in particular the support of
Austrian Federal Ministry of Education, Science and Culture, GZ 616.364/2-III/2a/98,
FNRS–FWO, Flanders Institute to encourage scientific and technological research in the industry (IWT), Belgium,
FINEP, CNPq, CAPES, FUJB and FAPERJ, Brazil,
Czech Ministry of Industry and Trade, GA CR 202/99/1362,
Commission of the European Communities (DG XII),
Direction des Sciences de la Matière, CEA, France,
Bundesministerium für Bildung, Wissenschaft, Forschung und Technologie, Germany,
General Secretariat for Research and Technology, Greece,
National Science Foundation (NWO) and Foundation for Research on Matter (FOM), The Netherlands,
Norwegian Research Council,
State Committee for Scientific Research, Poland, SPUB-M/CERN/PO3/DZ296/2000, SPUB-M/CERN/PO3/DZ297/2000, 2P03B 104 19 and 2P03B 69 23(2002-2004)
JNICT–Junta Nacional de Investigação Científica e Tecnológica, Portugal,
Vedecka grantova agentura MS SR, Slovakia, Nr. 95/5195/134,
Ministry of Science and Technology of the Republic of Slovenia,
CICYT, Spain, AEN99-0950 and AEN99-0761,
The Swedish Natural Science Research Council,
Particle Physics and Astronomy Research Council, UK,
Department of Energy, USA, DE-FG02-01ER41155.

References

[1] N. Bingefors et al., Nucl. Instr. and Meth. **A328** (1993) 447.

[2] V. Chabaud et al., Nucl. Instr. and Meth. **A368** (1996) 314.
[3] P. Chochula et al., Nucl. Instr. and Meth. **A412** (1998) 304.
[4] A. Andreazza et al., Nucl. Instr. and Meth. **A367** (1995) 198.
W. Adam et al., Nucl. Instr. and Meth. **A 379** (1996) 401.
[5] P.Collins, *The Alignment and Performance of the DELPHI Double-Sided Vertex Detector*, Proceedings of the fourth International Workshop on Vertex Detectors, June 1995, Ein Gedi Resort, Dead Sea, Israel, p. 13.
[6] ALEPH Collaboration, Phys. Lett. **B313** (1993) 535.
[7] DELPHI Collaboration, Nucl. Instr. and Meth. **A378** (1996) 57.
[8] DELSIM reference Manual, DELPHI 87-98 PROG 100, Geneva, 1989
[9] DELANA User's Guide, DELPHI 89-44 PROG 137, Geneva, 1989
[10] G. Borisov and C. Mariotti, Nucl. Inst. Meth. **A372** (1996) 181.
[11] ALEPH Collaboration, Phys. Lett. **B401** (1997) 150 and 163.
[12] SLD Collaboration, Phys. Rev. Lett. **80** (1998) 660.
[13] G. Borisov, Nucl. Instr. and Meth. **A417** (1998) 384.
[14] DELPHI Collaboration, E. Phys. J. **C10** (1999) 415.
[15] T.W. Anderson, An introduction to multivariate analysis, Wiley, New York, 1958.
[16] T. Sjöstrand, Comp. Phys. Comm. **39** (1986) 347; T. Sjöstrand, `PYTHIA 5.6` *and* `JETSET 7.3`, CERN-TH/6488-92; see also *Physics at LEP2*, G. Altarelli, T. Sjöstrand and F. Zwirner (eds.) CERN 96-01 (1996) Vol. 2, 41.
[17] DELPHI Collaboration, Z.Phys. **C73** (1996) 11.
[18] A. Ballestrero *et al.*, *Report of the QCD Working Group*, hep-ph/0006259;
S. Jadach, G. Passarino and R. Pittau (eds.) CERN 2000-009 (2000), 137.
[19] E. Norrbin and T. Sjöstrand, Nucl. Phys. **B603** (2001) 297.
[20] G. Rodrigo, Nucl. Phys. Proc. Suppl. **54A** (1997) 60;
G. Rodrigo, M. Bilenky and A. Santamaría, Nucl. Phys. **B554** (1999) 257.
[21] The LEP/SLD Heavy Flavour Working Group, *Final input parameters for the LEP/SLD heavy flavour analyses*, LEPHF/2001-01
[22] DELPHI Collaboration, Phys. Lett. **B462** (1999) 425.
[23] DELPHI Collaboration, Phys. Lett. **B425** (1998) 399.
[24] S. Catani et al., Phys. Lett. **B269** (1991) 432;
N. Brown and W. J. Stirling, Z. Phys. **C53** (1992) 629.
[25] Yu. L. Dokshitzer, G. D. Leder, S. Moretti and B. R. Webber, JHEP 9708:001 (1997), hep-ph/9707323.
[26] DELPHI Collaboration, Phys. Lett. **B418** (1998) 430;
S. Martí i García, J. Fuster and S. Cabrera, Nucl. Phys. **B** (Proc. Suppl.) **64** (1998) 376.
[27] DELPHI Collaboration, Phys. Lett. **B499** (2001) 23.

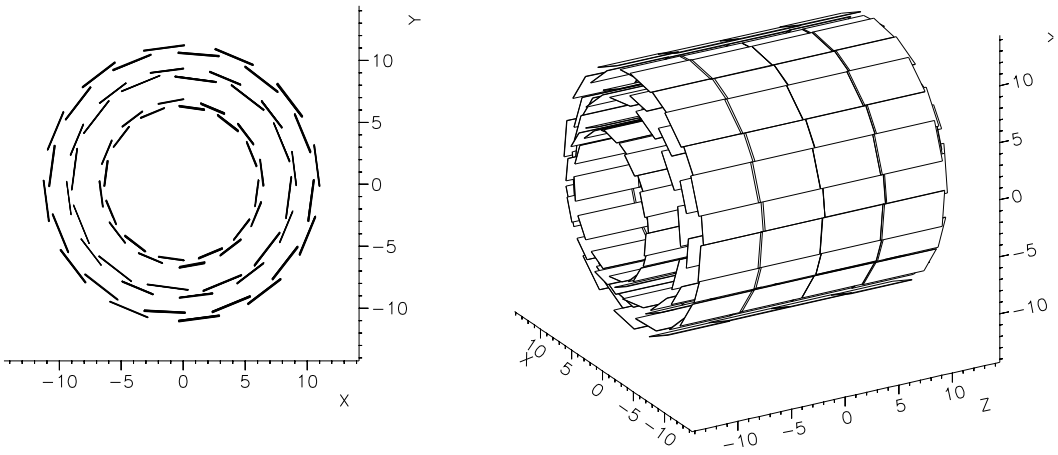

Figure 1: Schematic cross sections of the Double Sided Vertex Detector in **(a)** the transverse ($R\phi$) view and **(b)** a three-dimensional view. Dimensions are in cm.

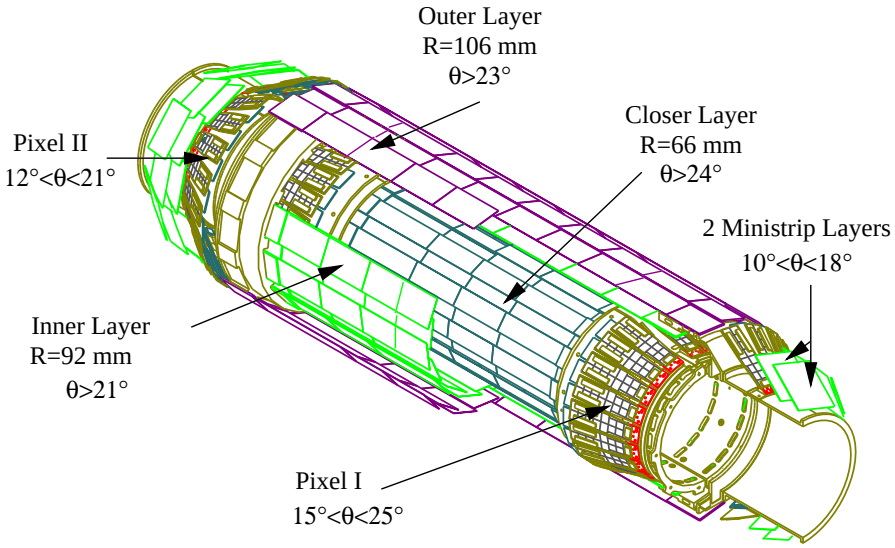

Figure 2: Schematic view of the Silicon Tracker

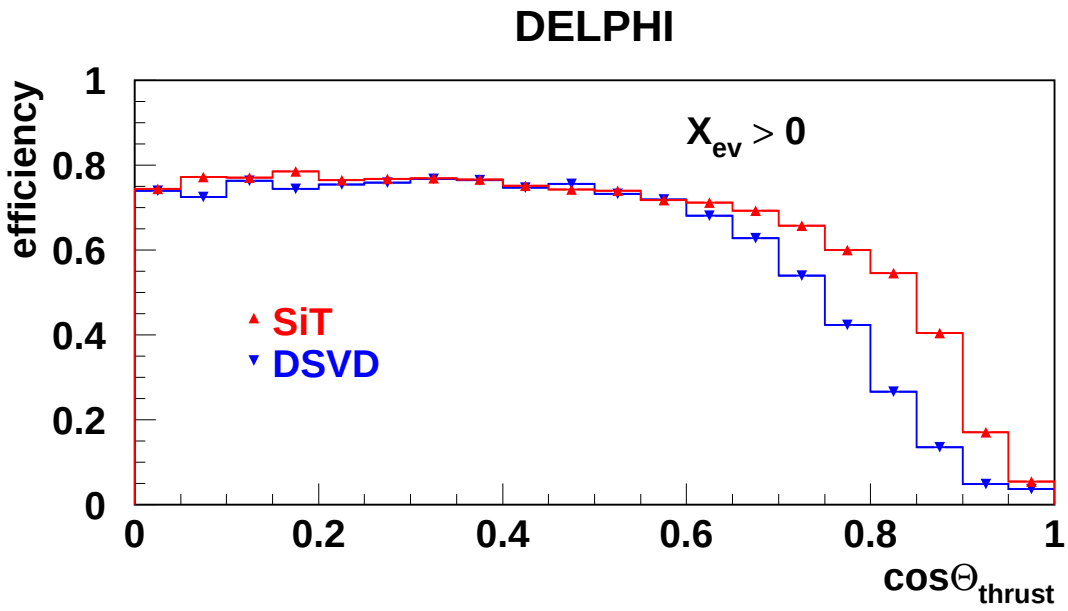

Figure 3: Selection efficiency of $Z \to b\bar{b}$ events versus $\cos\Theta_{thrust}$ using the combined event b-tagging variable $X_{ev} > 0$ for the Silicon Tracker and the Double Sided Vertex Detector. (X_{ev} is defined in Section 4.1.) The extra coverage provided by the Silicon Tracker in the forward direction is clearly visible.

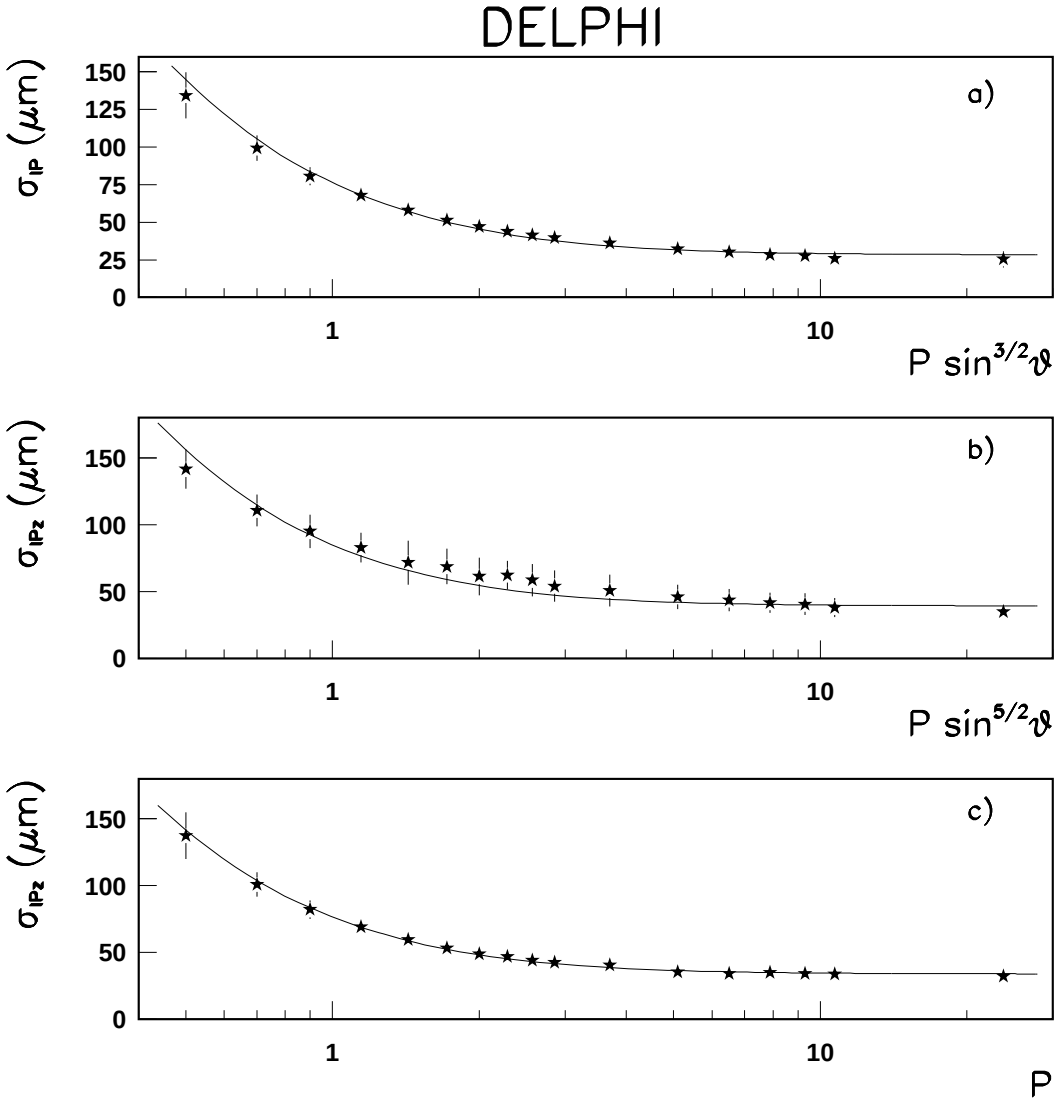

Figure 4: The $R\phi$ IP uncertainty as a function of p $\sin^{\frac{3}{2}}\theta$ (upper plot), the Rz IP uncertainty as a function of p $\sin^{\frac{5}{2}}\theta$ (middle plot) and the Rz IP uncertainty as a function of p for tracks with $\theta = [80^\circ : 100^\circ]$, i.e. perpendicular to the beam direction (lower plot). The data are from the Double Sided Vertex Detector at the Z. The curves are parameterisations of a constant intrinsic resolution term and a momentum-dependent multiple scattering contribution. Momenta are in Gev/c.

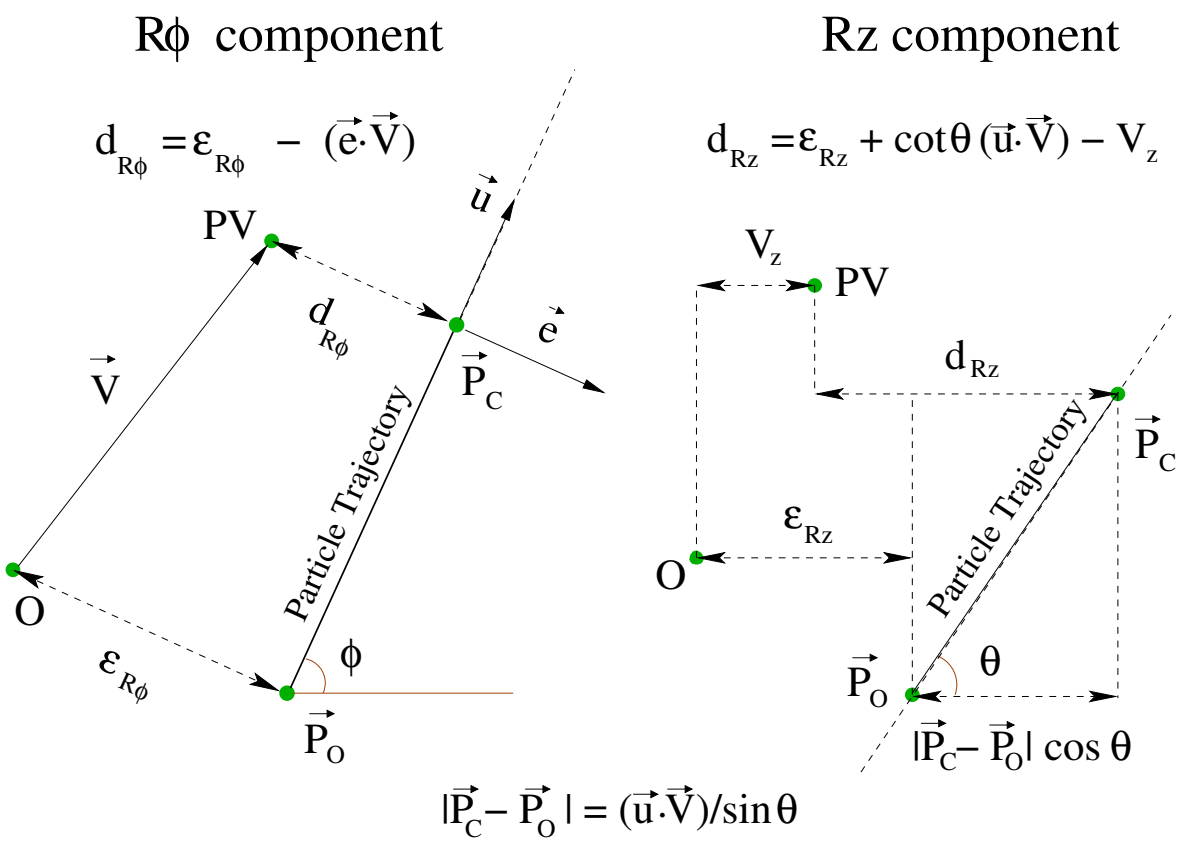

Figure 5: Definition of $R\phi$ and Rz IP components. $\overrightarrow{u}$ is a unit vector along the track direction, and $\overrightarrow{e}$ is another unit vector in the $R\phi$ plane, perpendicular to $\overrightarrow{u}$. $\overrightarrow{V}$ is a vector from the origin O to the primary vertex PV. P_0 and P_C are the points of closest approach in the $R\phi$ plane of the track trajectory to O and to PV respectively. The diagrams show the projections onto the $R\phi$ and Rz planes. The IP components are $d_{R\phi}$ and d_{Rz}, while $\varepsilon_{R\phi}$ and ε_{Rz} are the corresponding components from P_0 to the origin.

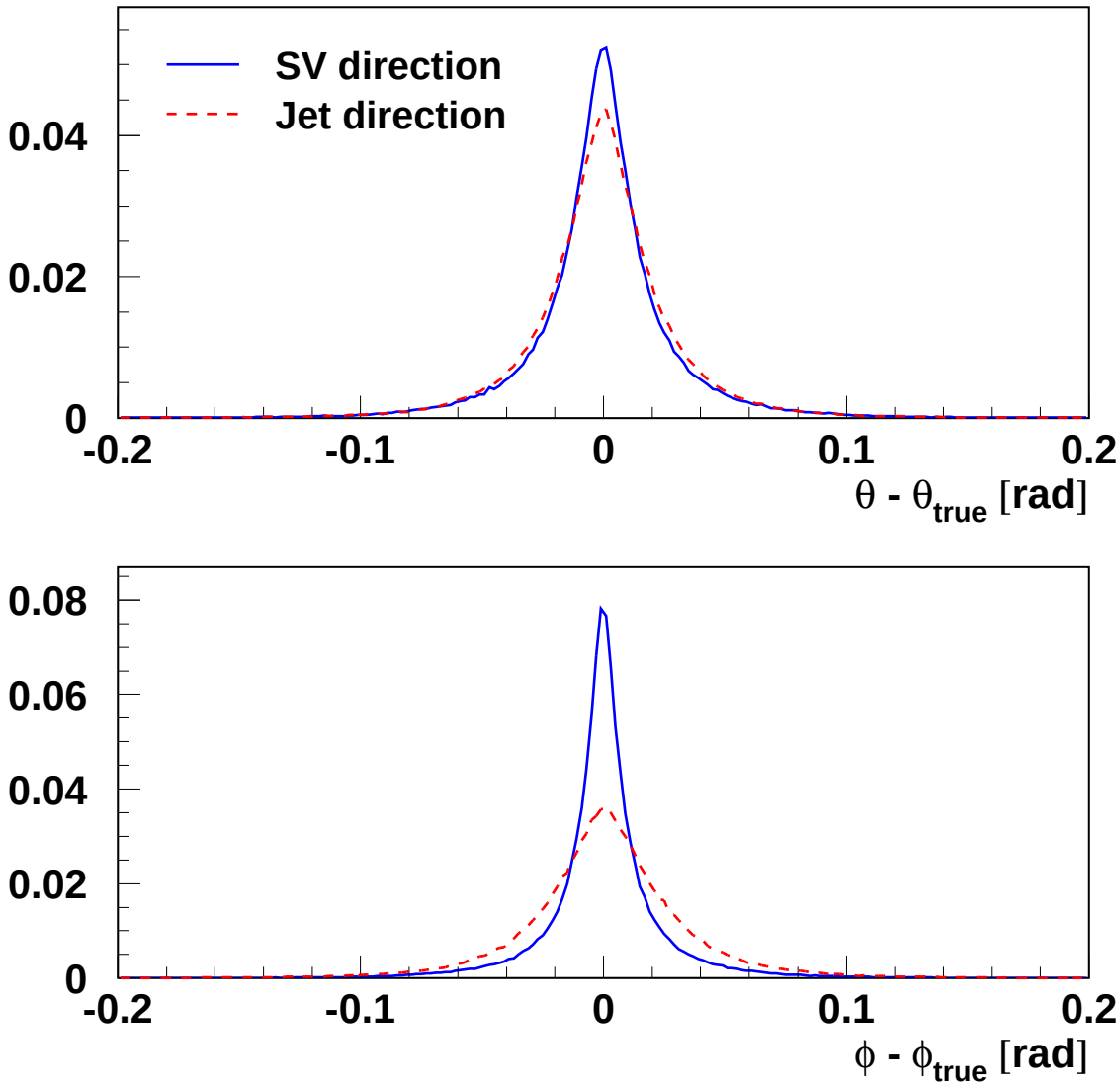

Figure 6: Distributions of the difference between reconstructed and generated directions of b-hadrons for events with a reconstructed secondary vertex, for simulated Z events. The B direction is defined as the direction from the primary to the secondary vertex (solid line) or as the jet direction (dashed line). Especially in ϕ, the definition using the secondary vertex gives a better description of the B direction.

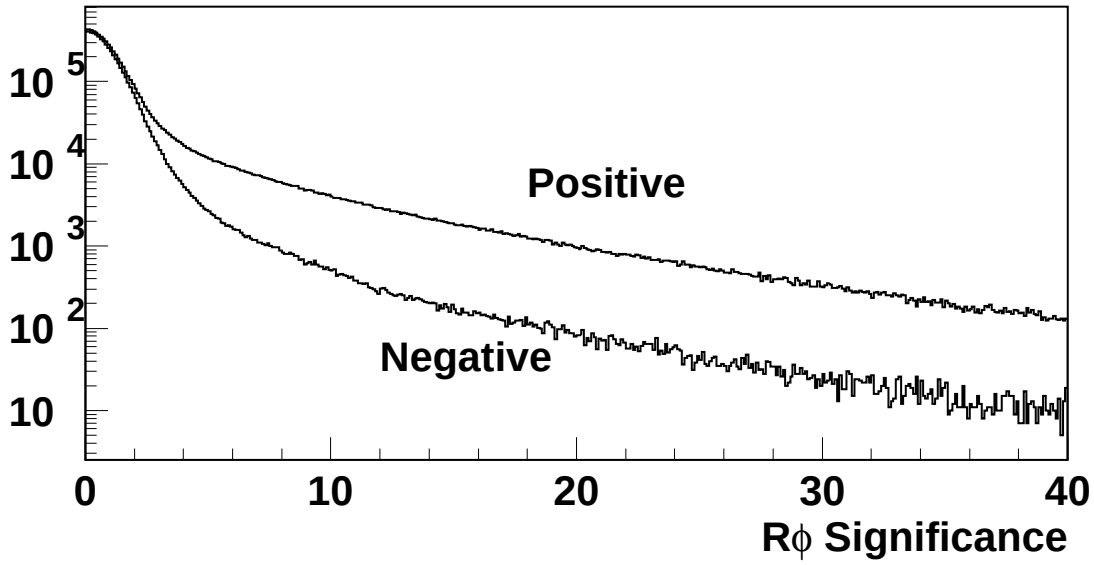

Figure 7: Distributions of positive and negative $R\phi$ significances in data Z hadronic decays. The excess of tracks with large positive significance is due to long-lived particles.

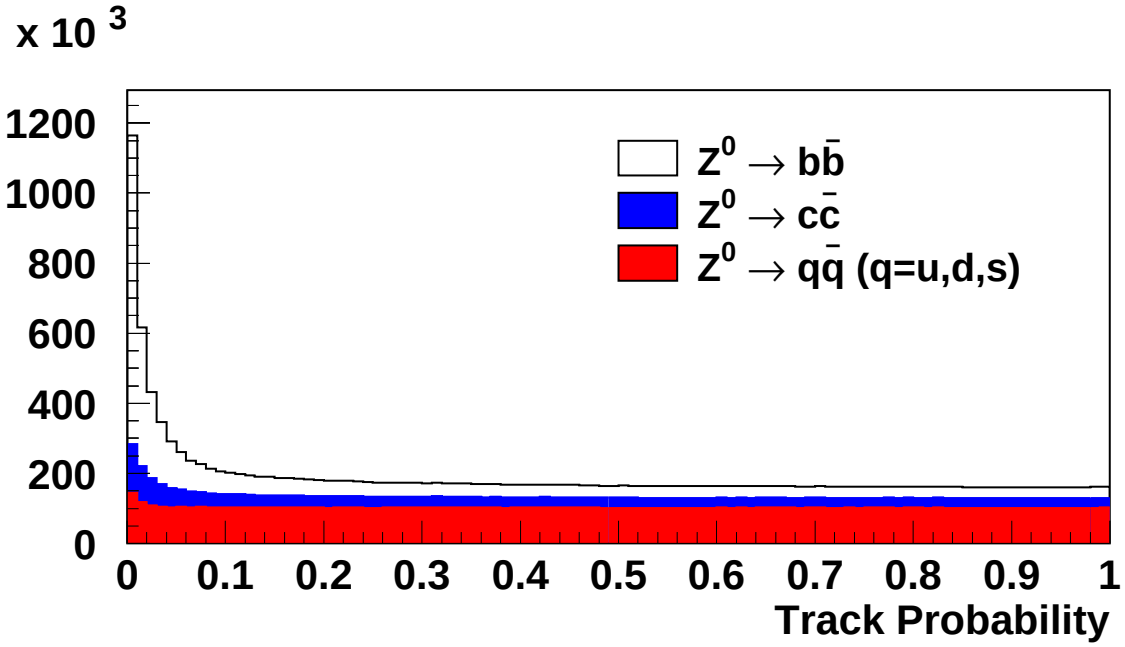

Figure 8: Simulated distributions at the Z of the $R\phi$ track IP probabilities for different quark flavours, for tracks with positive lifetime-sign IPs.

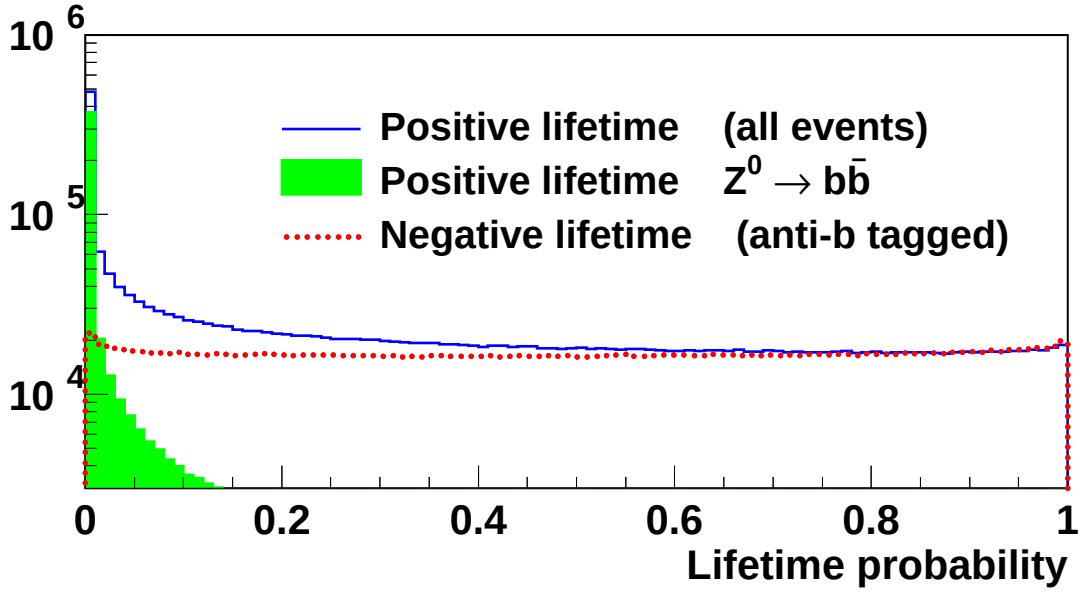

Figure 9: Distributions of positive and negative lifetime probabilities (P_N^+ and P_N^- respectively) for simulated Z hadronic events.

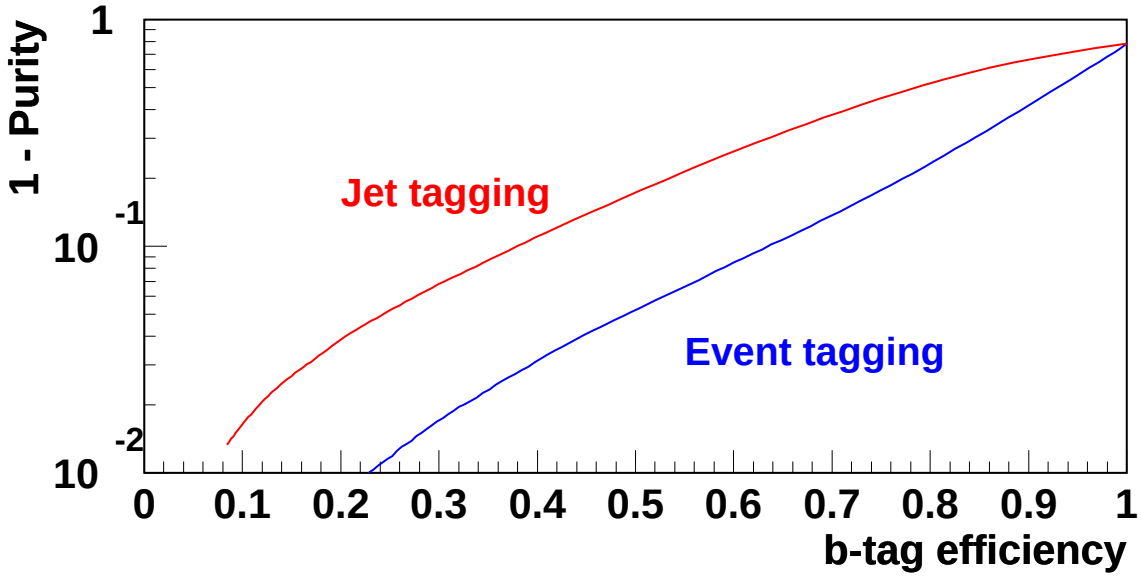

Figure 10: Background suppression in simulated Z hadronic events using lifetime tagging. The efficiency is the fraction of b-jets that are tagged as coming from b-quarks, while the purity is the fraction of tagged jets that are really from b-quarks.

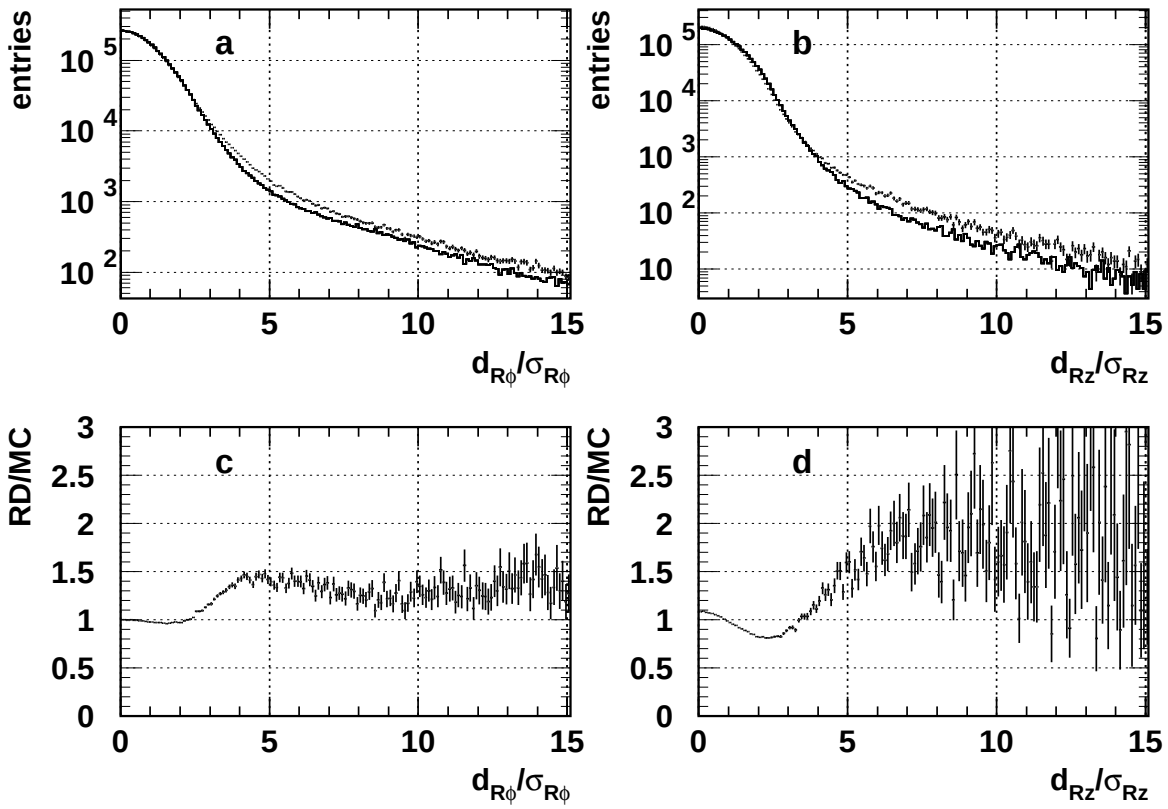

Figure 11: **a)** and **b)** The $R\phi$ and Rz significance distributions for tracks with negative IP. The points with errors are real data, the histogram is simulation. **c)** and **d)** The ratios of these distributions (data divided by simulation).

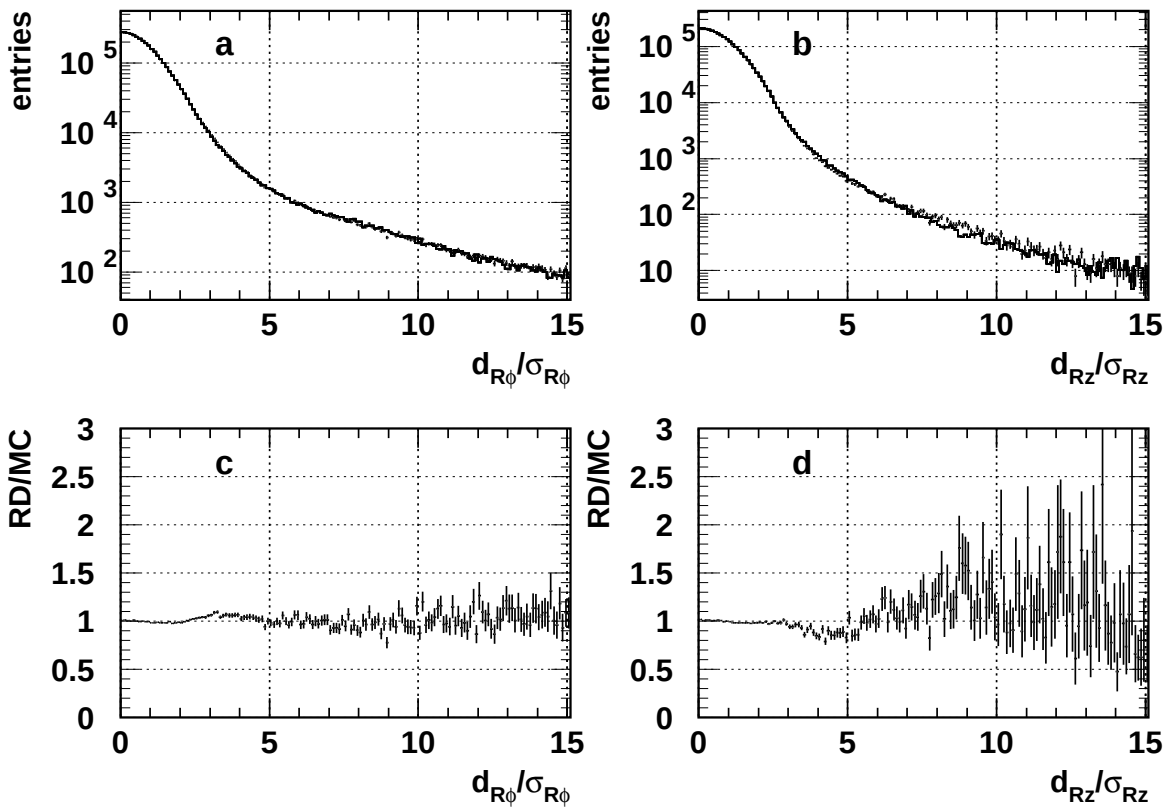

Figure 12: **a)** and **b)** The $R\phi$ and Rz significance distributions for tracks with negative IP after the tuning procedure. The points with errors are real data, the histogram is simulation. **c)** and **d)** The ratios of these distributions (data divided by simulation). The improvement resulting from tuning is clearly visible.

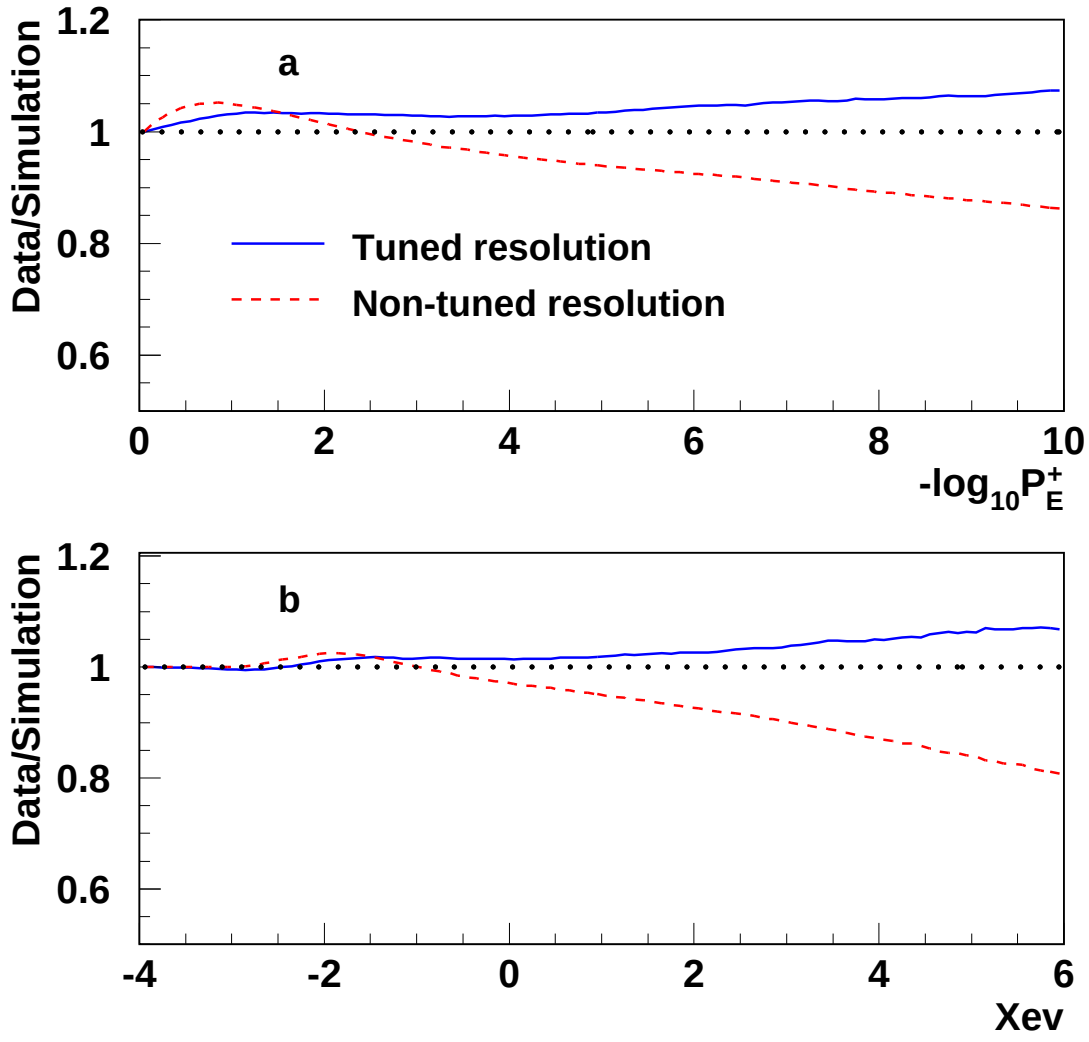

Figure 13: The integrated data to simulation ratio of the fraction of selected hemispheres as a function of the cut on the b-tagging variable for **a)** the lifetime tagging variable P_E^+, calculated using all positive lifetime IP tracks in an event (see Section 3.5) and **b)** combined tagging variable X_{ev}(see Section 4), with tuned (full line) and non-tuned (dashed line) track resolution.

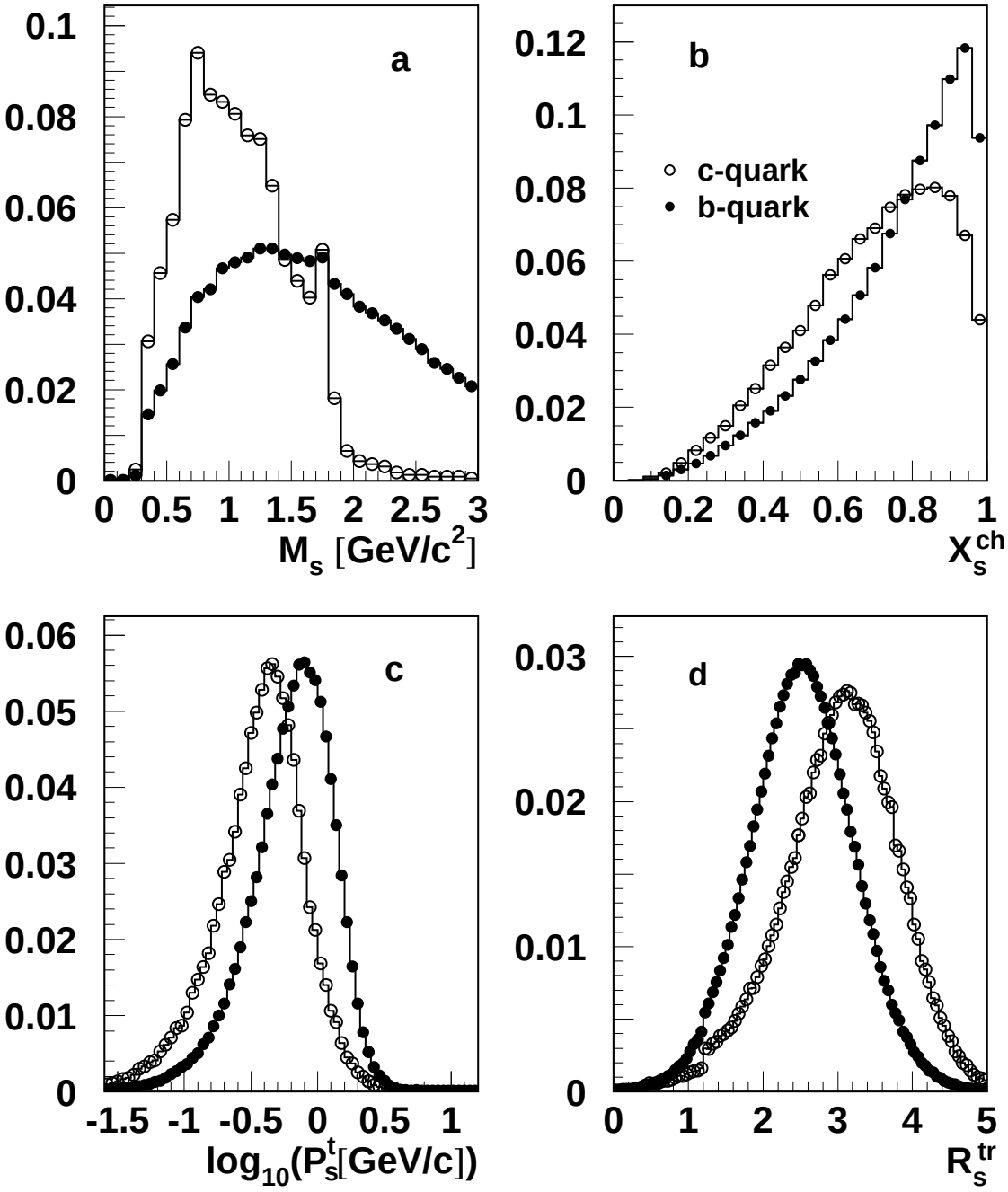

Figure 14: Distributions of discriminating variables for b- and c- quark jets for simulated Z hadronic events. **a)** Mass of particles in SV. **b)** Fraction of charged jet energy included in SV. **c)** Transverse momentum at SV. **d)** Rapidity for each SV track.

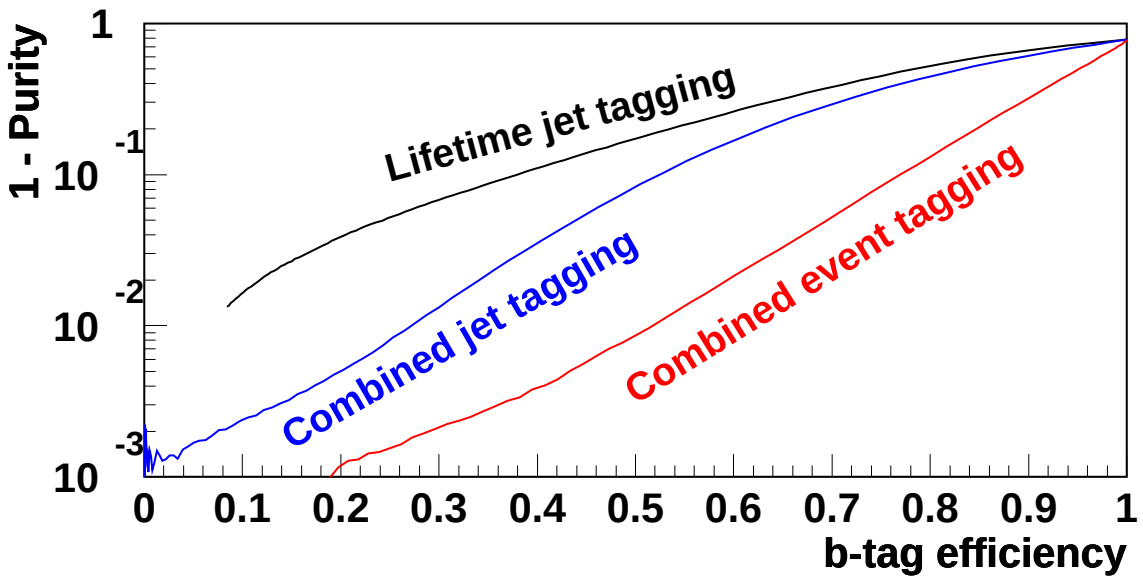

Figure 15: Background suppression in Z hadronic events using combined b-tagging.

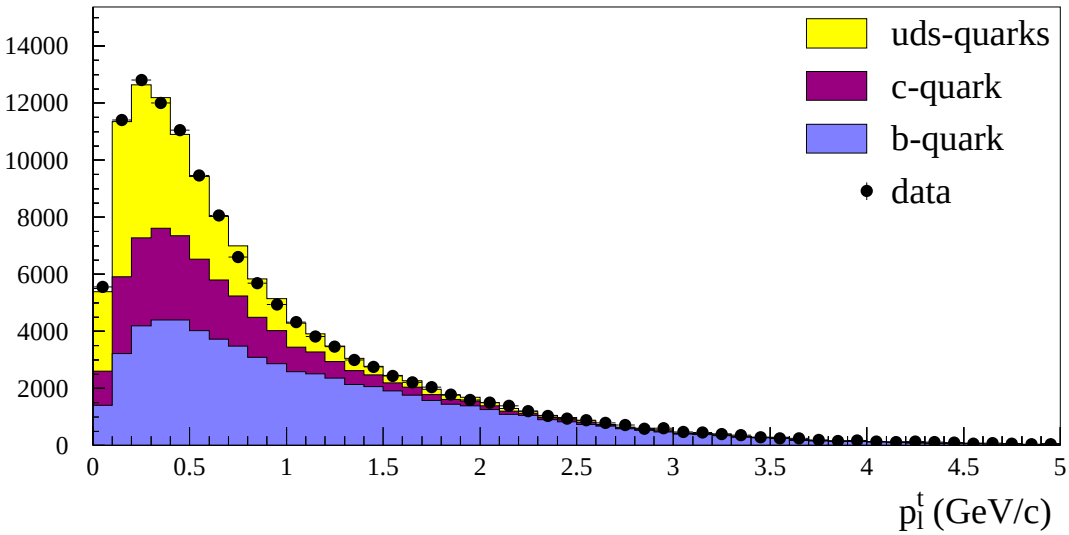

Figure 16: Transverse momentum distribution of identified leptons with respect to the jet from which they originate, measured in hadronic Z decays at LEP1. The contributions from light quarks, c-quarks and b-quarks are added and compared to the data.

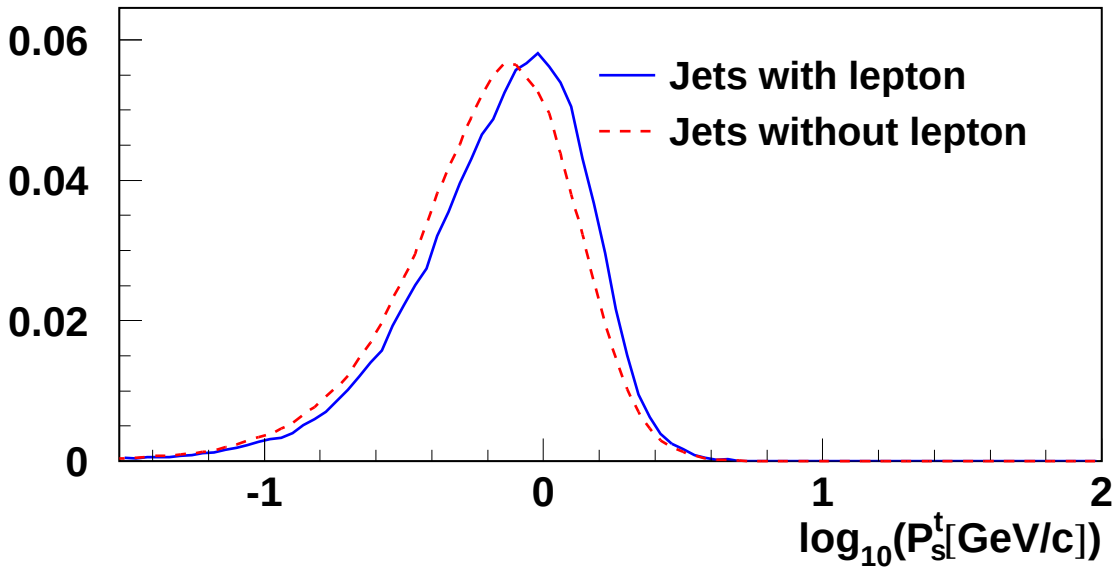

Figure 17: Distribution of $\log_{10}(P_s^t)$ for jets with (solid line) and without (dashed line) leptons.

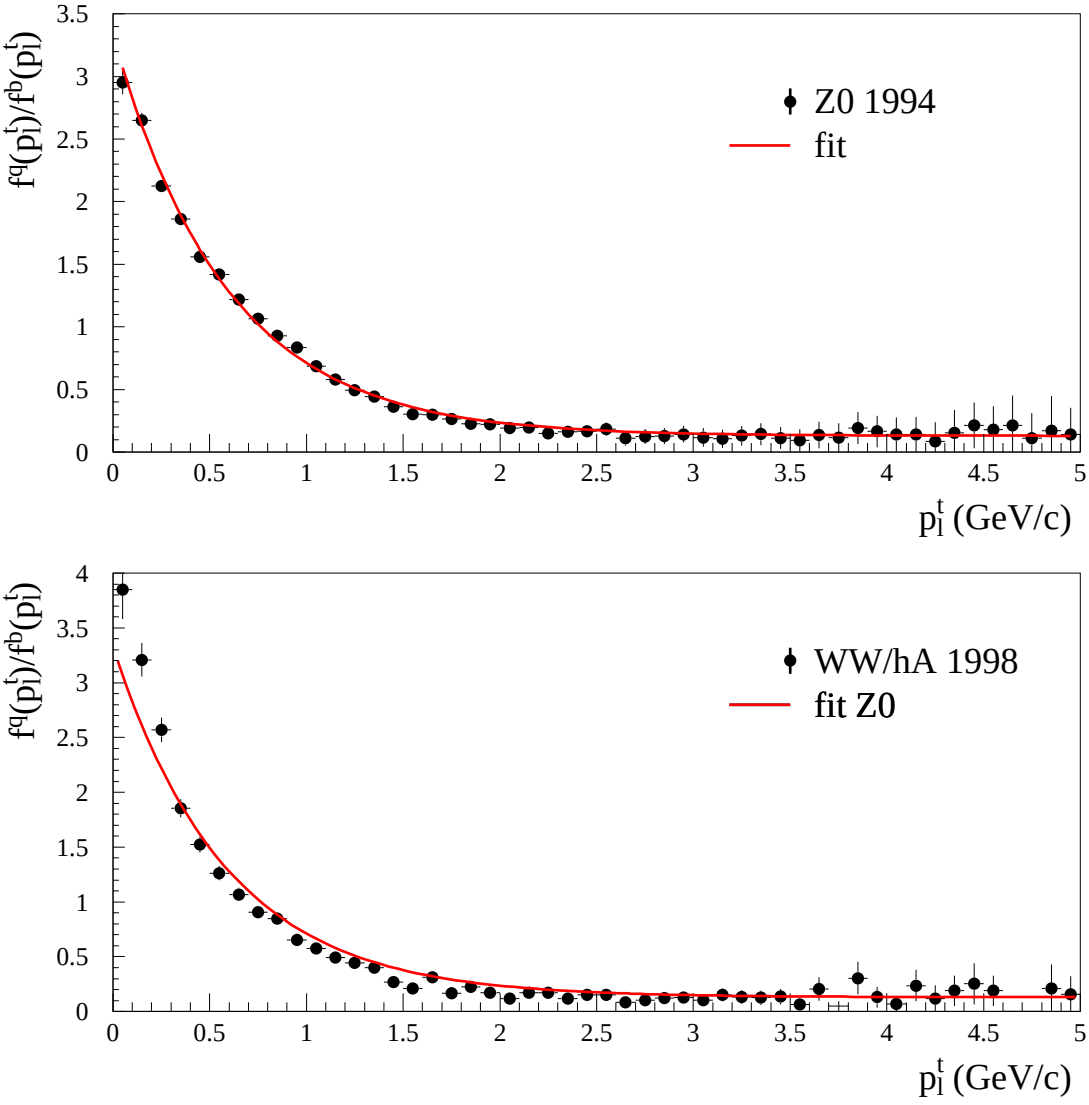

Figure 18: The upper figure shows the ratio of the numbers of light-quark and b-quark events as a function of the lepton transverse momentum (dots), as extracted from simulated hadronic Z decays. The line is the fit to that ratio. The lower figure shows the same ratio, extracted from a simulated Higgs signal and WW background at LEP2. The line is the Z fit.

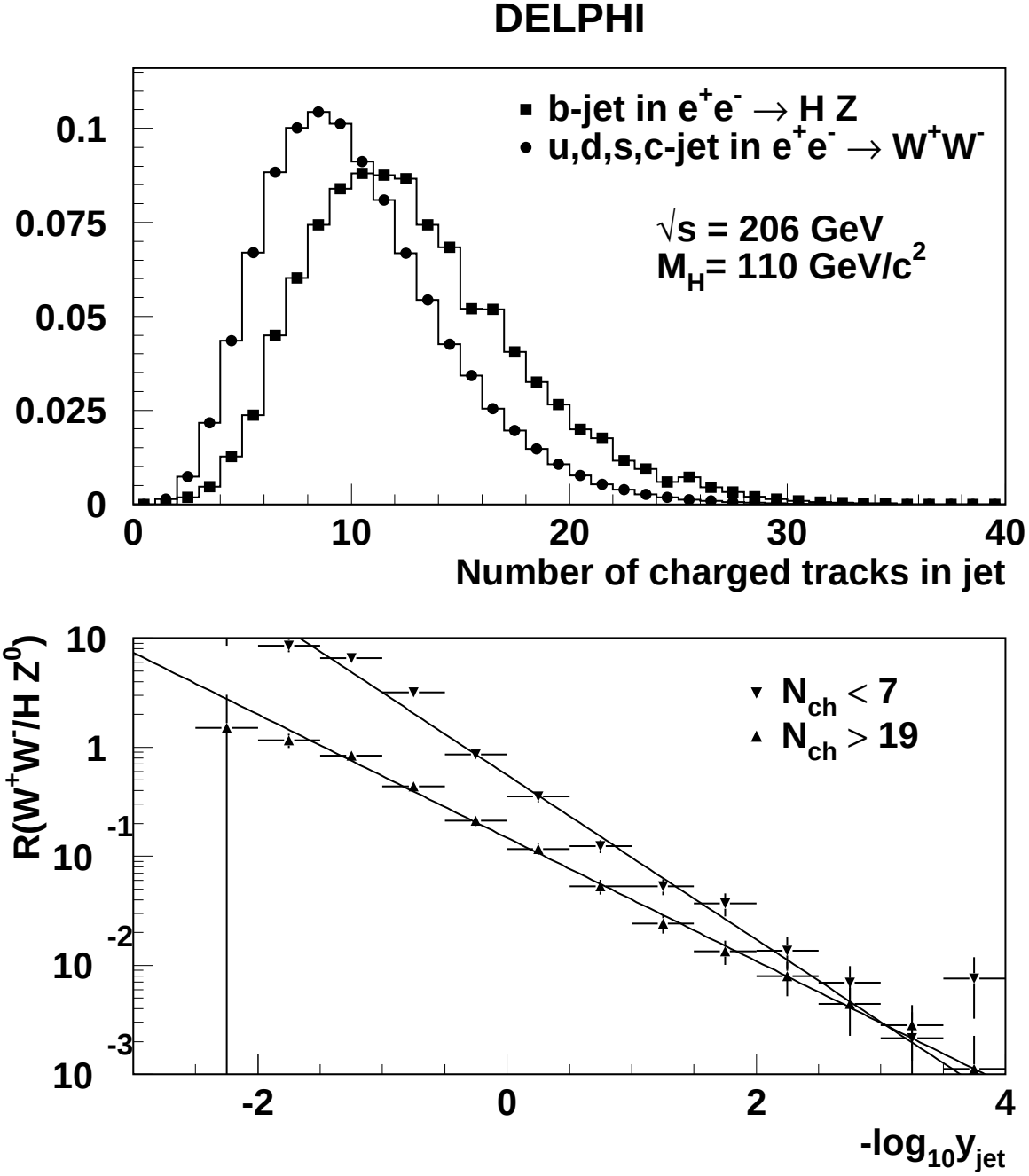

Figure 19: Upper plot: Simulated distributions of the number of tracks in a b-jet from the $e^+e^- \to HZ$ process and in a light quark jet from the $e^+e^- \to W^+W^-$ process. Lower plot: the ratio $R(W^+W^-/HZ)$ of the number of light quark jets from the $e^+e^- \to W^+W^-$ process to that of b-jets from $e^+e^- \to HZ$ process in the simulation (arbitrary normalisation) as a function of $-\log_{10} y_{jet}$, shown separately for jets with less than 7 or greater than 19 tracks. The lines in each case show the exponential fit of these rates.

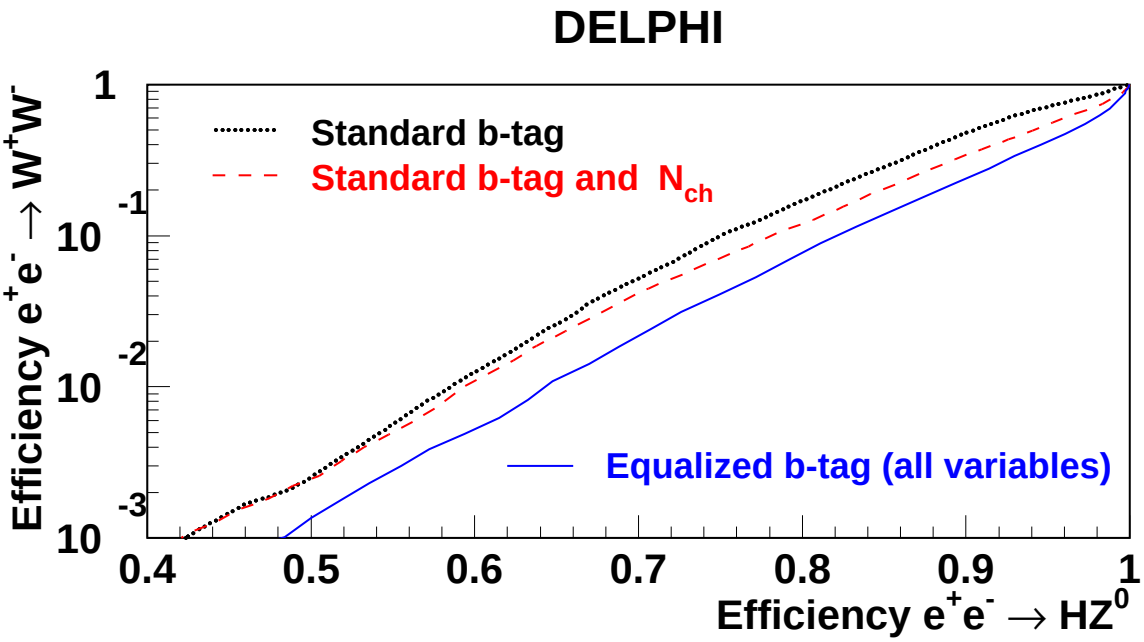

Figure 20: Mis-tagging efficiency for $e^+e^- \to W^+W^-$ versus $e^+e^- \to HZ$ selection efficiency, as obtained from standard combined b-tagging, b-tagging equalised with respect to N_{ch}, and equalised b-tagging with the complete set of variables (see text for details).

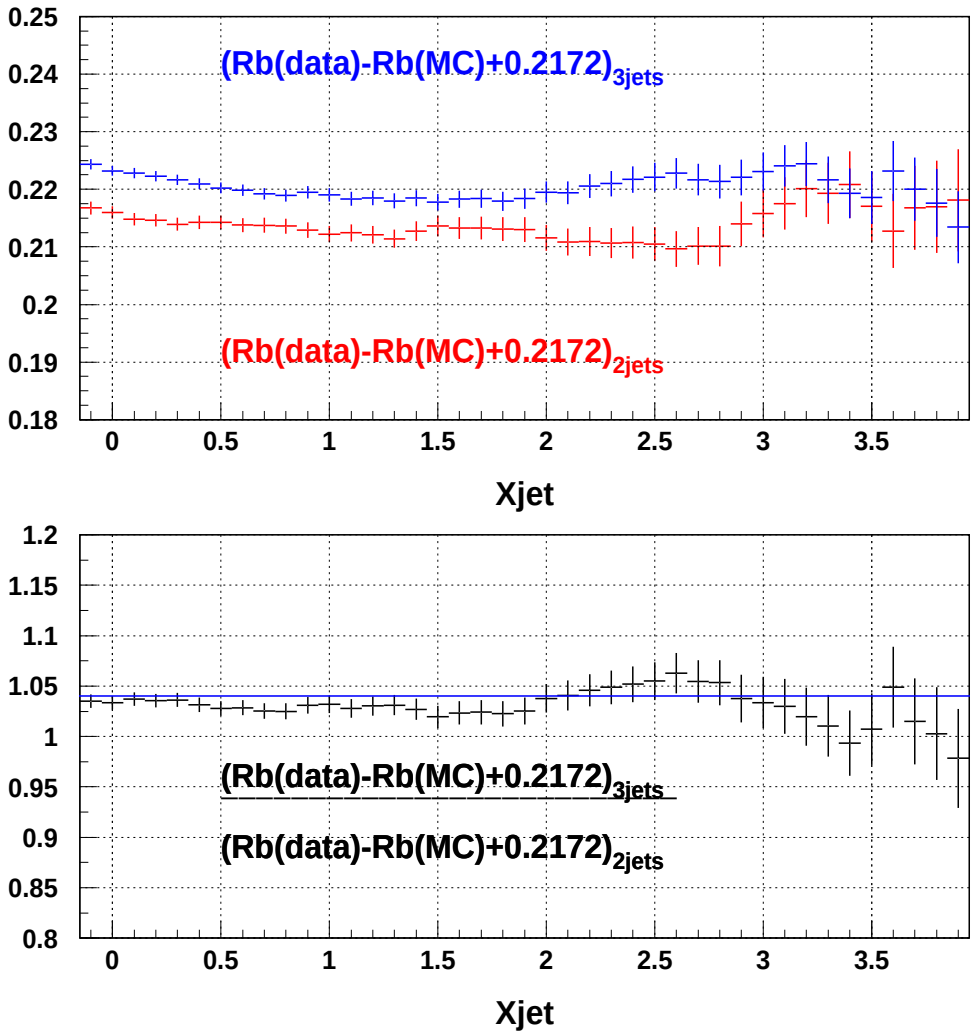

Figure 21: Comparison of the measurements of the R_b ratio in 2 and 3 jet events at the Z, as a function of the cut in the b-tagging variable X_{jet}. The simulation used `JETSET 7.4`.

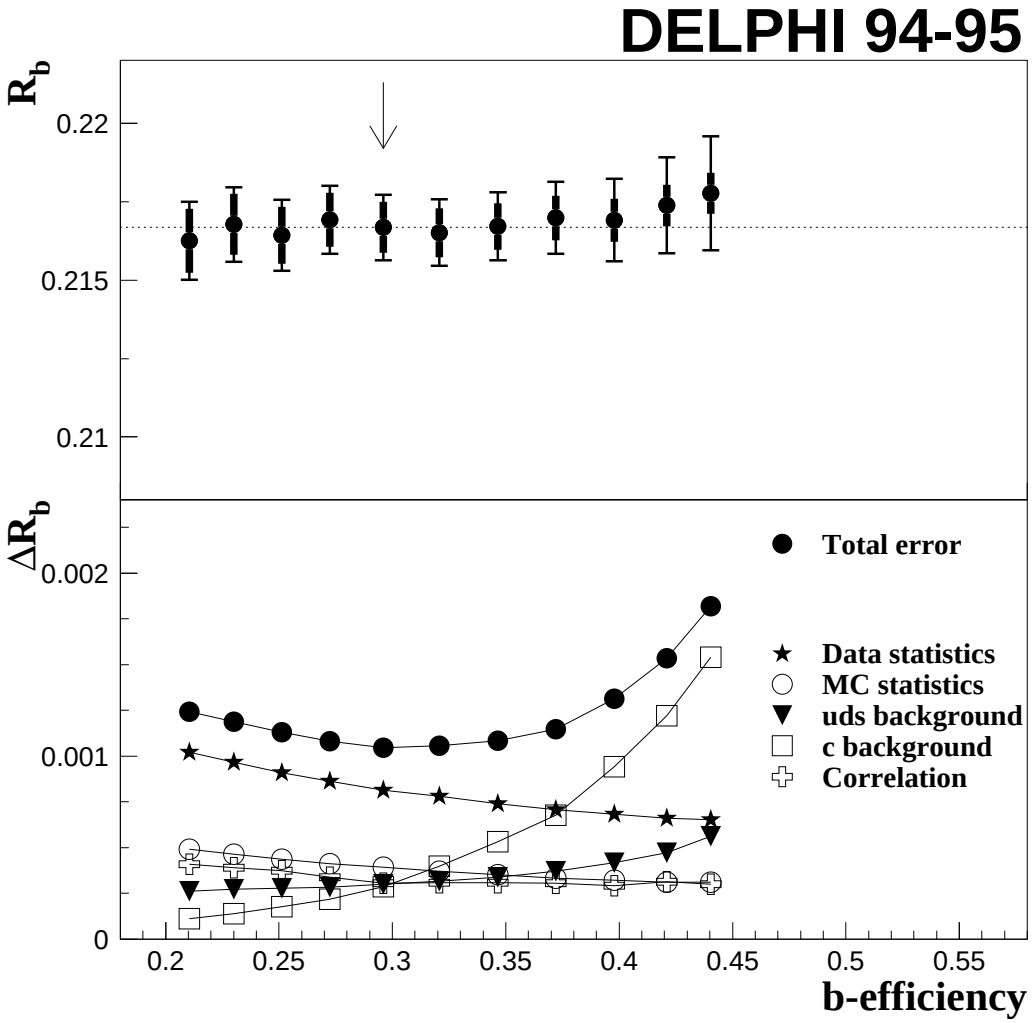

Figure 22: Stability of the R_b result as a function of the b-tagging efficiency, for data collected in 1994–5. The arrow shows the b-efficiency chosen for the final result.

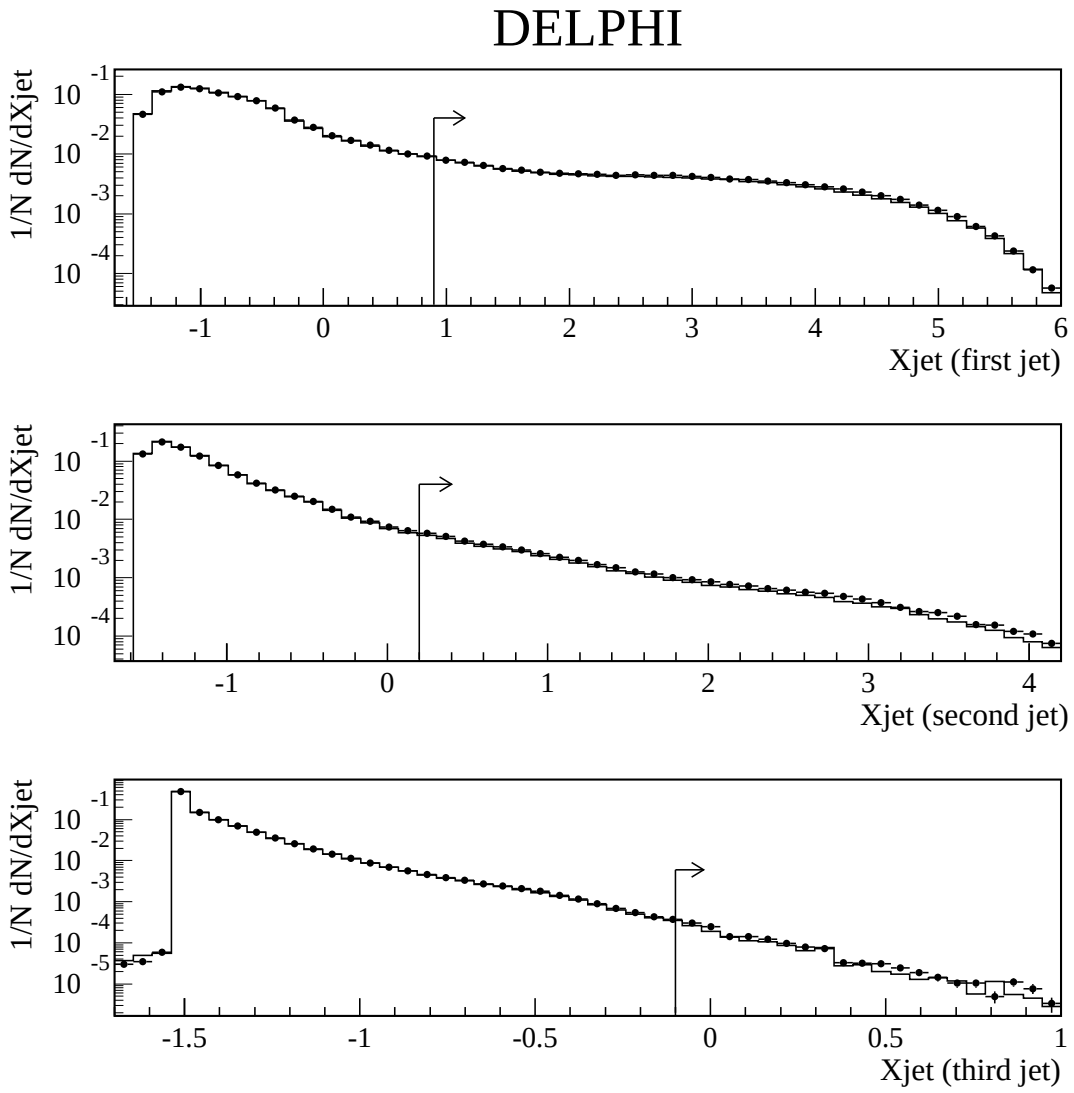

Figure 23: Distribution of the b-tagging variables for the first three jets, ordered according to their b-tagging variable, for Z data (dots) and simulation (histogram). The arrows show the positions of the cuts used to select the b jets. The figure is from reference [22].

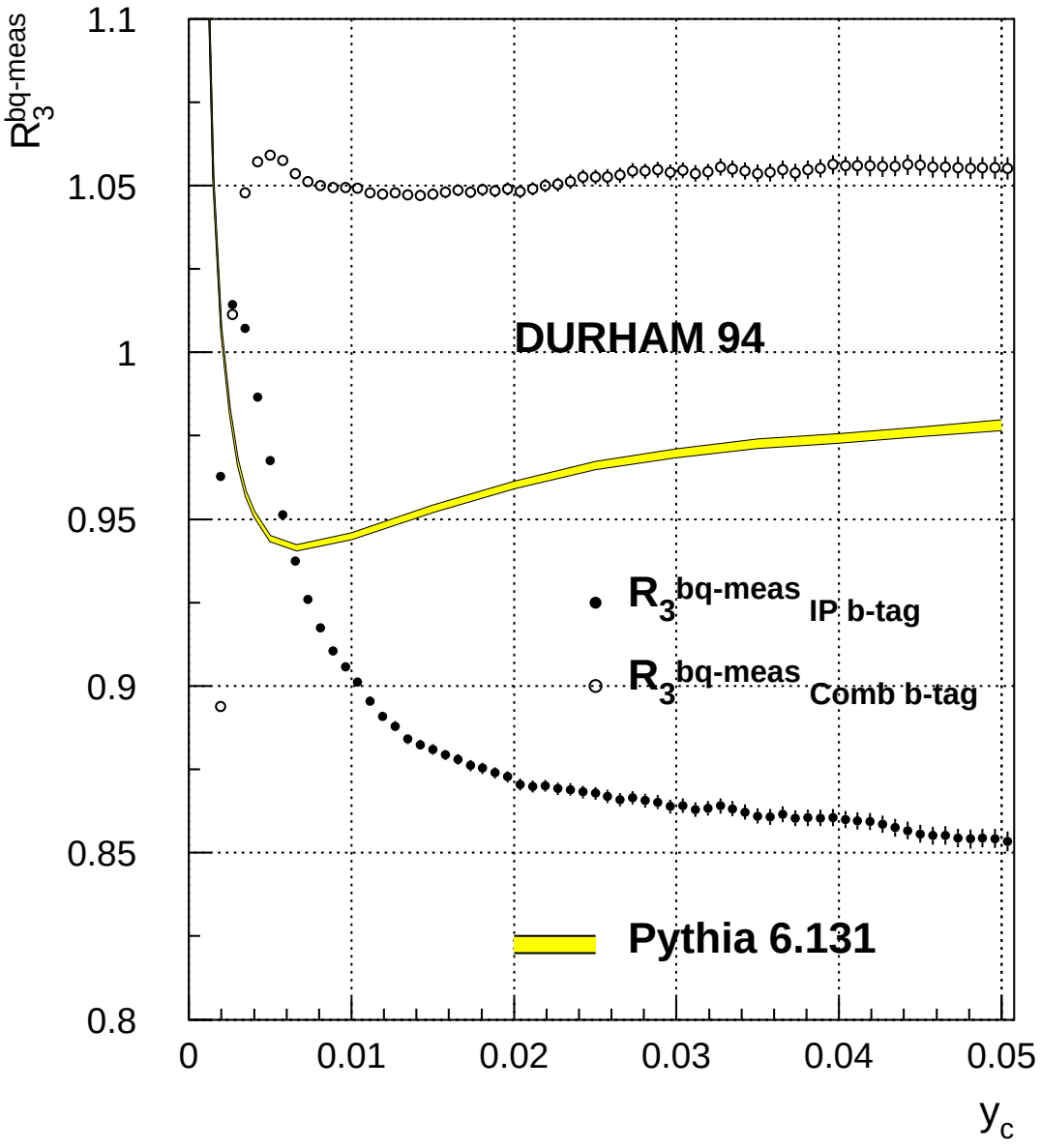

Figure 24: The $R_3^{bq-meas}$ observable from simulated DELPHI data for the two tagging techniques and the parton level $R_3^{bq-part}$ obtained with PYTHIA 6.131. The DURHAM jet finding algorithm is used.

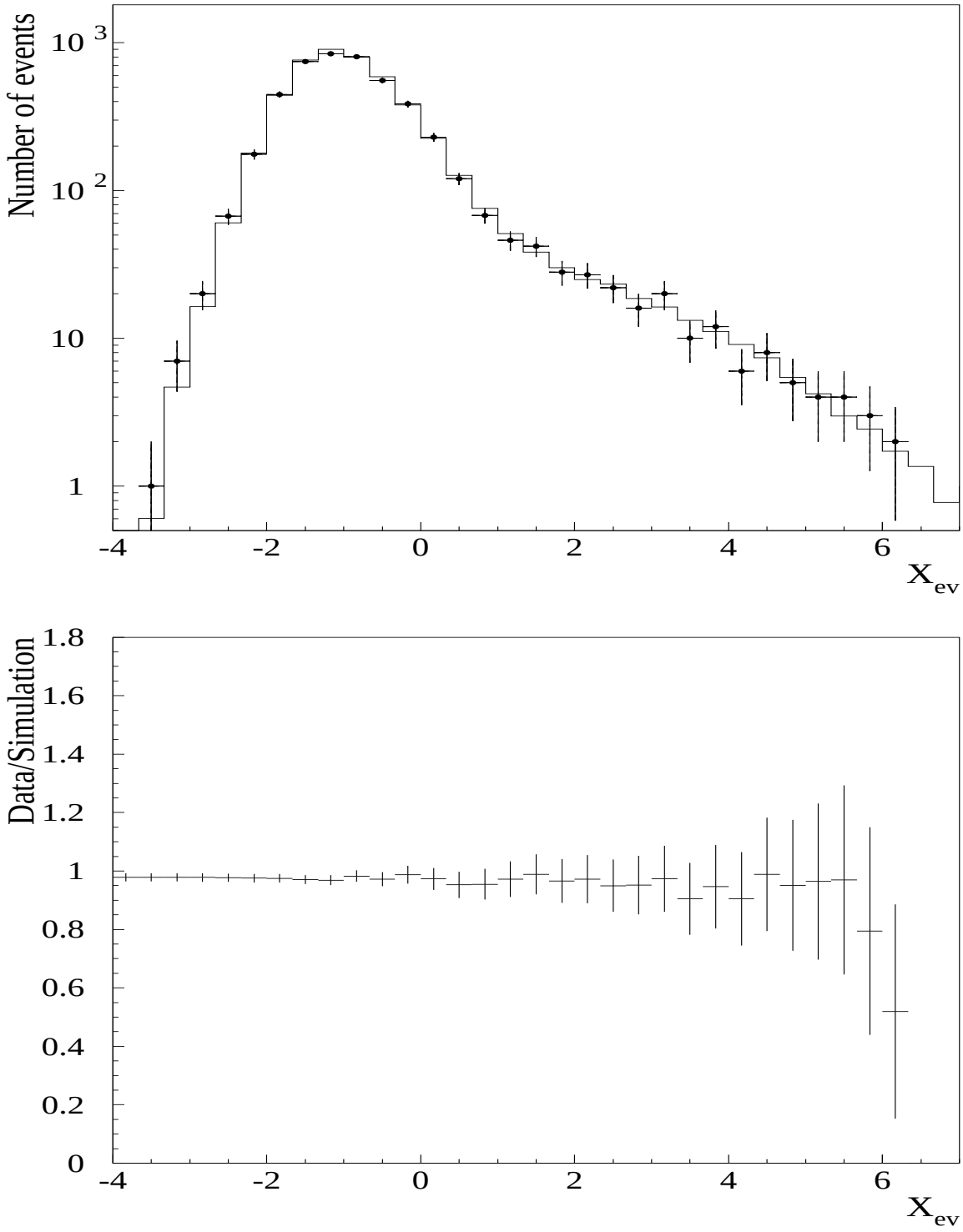

Figure 25: Top: distribution of the equalised b-tagging variable for 4-jet events at $\sqrt{s} = 192 - 210$ GeV, data (dots) and simulation (solid line). Bottom: ratio of the integrated tagging rates in data and simulation as a function of the cut in the equalised b-tagging variable. The agreement between data and simulation is satisfactory.

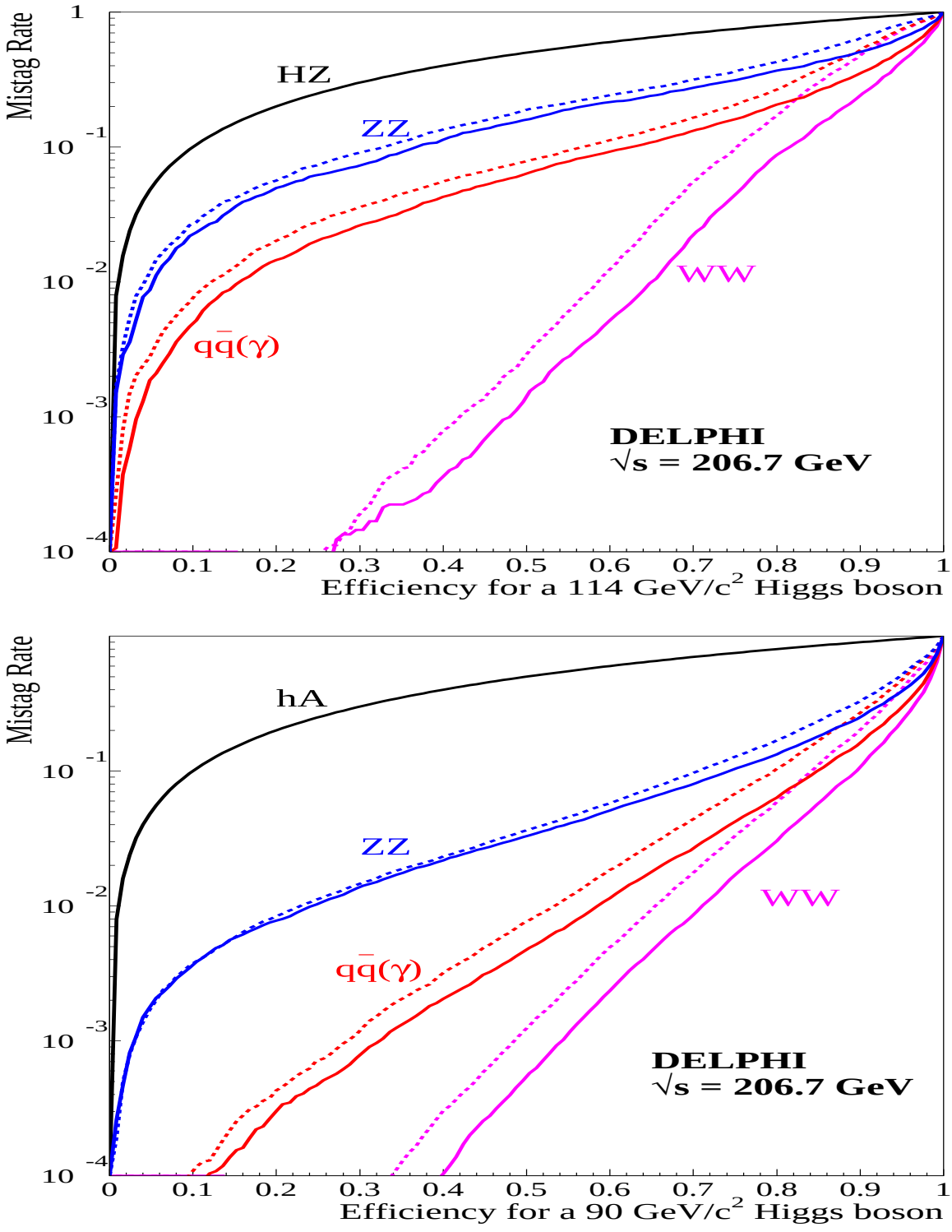

Figure 26: Expected SM background mis-tag rates at $\sqrt{s} = 206.7$ GeV, as functions of the signal efficiency for a Standard Model Higgs boson of mass 114 GeV/c^2 (top) and MSSM Higgs boson of mass 90 GeV/c^2 and $\tan\beta = 20$ (bottom) when varying the cut on the equalised b-tagging variable (solid lines) and combined b-tagging variable (dotted lines).